

# Decomposing Evolutionary Mixture-of-LoRA Architectures: The Routing Lever, the Lifecycle Penalty, and a Substrate-Conditional Boundary

Ramchand Kumaresan

Murai Labs

*mechramc@gmail.com*

Reviewed on OpenReview: <https://openreview.net/forum?id=XXXX>

## Abstract

We decompose an evolutionary mixture-of-LoRA system on a from-scratch  $\sim 150\text{M}$ -parameter widened- $D$  substrate ( $D=1536$ ,  $V=32000$ ;  $D/V \approx 0.048$ ; we refer to this as the “widened-1536” substrate) into three factors — a router rewrite (parallel sigmoid gate with learnable per-adapter floor and bounded temperature anneal, fed post-stack hidden states rather than token-embedding means), a per-domain leave-one-out evaluation scope, and a lifecycle of death plus  $\alpha$ -blend inheritance plus SVD mutation plus slot reallocation — and report a 5-of-8 partial  $2^3$  factorial run at  $n=3$  seeds and 25000 adaptation steps per cell. The attribution chain is sharp on this substrate: the router rewrite carries the entire  $+0.0426$  nat balanced log-PPL improvement (under the convention  $\Delta = \log \text{PPL}_{\text{ref}} - \log \text{PPL}_{\text{test}}$ , positive = improvement;  $t=12.86$ ,  $p=0.006$ ) attributed to “the full evolutionary system vs the static B3 baseline” in our own internal numbers; the headline full-system-vs-B3 balanced contrast itself is  $+0.015$  nats,  $t=1.94$ ,  $p=0.19$  at  $n=3$  and does not clear  $\alpha=0.05$ . The per-domain evaluation scope is null at seed-resolution, and the lifecycle is a net drag of  $\approx -0.028$  nats ( $t=-4.46$ ,  $p=0.047$  in the primary chain). An auxiliary  $\alpha=0$  inheritance counterfactual at  $n=3$  seeds is sign-inconsistent at the headline metric and underpowered for either an equivalence or a load-bearing conclusion (an earlier draft of this paper claimed the counterfactual ruled out inheritance as the load-bearing source of the lifecycle penalty; that claim depended on an arithmetic-mean aggregator that, when corrected to the pinned geometric mean, flips the seed-42 cell to the load-bearing range and leaves the cross-seed mean inside the ambiguous band, see Appendix B.11). A base-perturbation probe directionally refutes a “genomic-context” reframe of the lifecycle role. A controllable synthetic sandbox locates a substrate-conditional regime boundary: evolutionary search on the routing channel is load-bearing only when adapters are pre-aligned to the task; in every other regime tested it underperforms, ties, or actively degrades the gradient solution.

## 1 Introduction

Modern parameter-efficient adaptation of large language models layers many low-rank adapters on top of a frozen backbone, often gated by a sparse mixture-of-experts router that selects a subset of adapters per input token (Hu et al., 2021; Li et al., 2024). A natural further step is to make the population of adapters itself *evolutionary*: adapters compete on a fitness signal, the worst adapters die, vacated slots are repopulated by mutated clones of the fittest, and a fraction of the dying adapter’s weights is blended into a nearest neighbor before slot release. The hypothesis underlying such an “evolutionary mixture-of-LoRA” design — that lifecycle dynamics (selection, reproduction, inheritance, mutation) produce better-organized adapter populations than static allocation — is plausible by analogy with neuroevolution and population-based training (Stanley et al., 2019; Jaderberg et al., 2017), but the empirical record on whether this analogy carries over to text-domain mixture-of-LoRA training has been thin. This paper supplies that empirical record on a single specific substrate, and reports a result that is more nuanced than either a clean win or a clean null.

**One-sentence contribution.** On a 5-of-8 partial  $2^3$  factorial decomposing an evolutionary mixture-of-LoRA system into three factors, the *router rewrite* factor carries the entire balanced-perplexity improvement over the static baseline, the *lifecycle* factor is a net drag, and the *evaluation-scope* factor is null at seed-resolution; the contribution decomposes into a routing lever, a lifecycle penalty, and a substrate-conditional regime boundary that we characterize first on a synthetic sandbox and then on the production run.

**What.** We report three concrete claims, each backed by a paired statistical test on three seeds:

- **The routing lever.** Replacing a softmax-over-adapters router (which on this widened-1536 substrate collapses onto a single 4-of-16 cross-domain adapter coalition; Jensen–Shannon divergence between per-domain top- $k$  gate distributions equals exactly 0) with a parallel-sigmoid router carrying a learnable per-adapter floor and a bounded temperature anneal, and feeding it post-stack hidden states rather than token-embedding means, accounts for the entire +0.0426 nat balanced log-PPL improvement ( $t=12.86$ ,  $p=0.006$ ) attributed to “the full evolutionary system vs the static B3 baseline” in our own internal numbers (Section 5).
- **The lifecycle penalty.** Death,  $\alpha$ -blend inheritance, SVD mutation, and slot reallocation, layered on top of the rewritten router, cost approximately 0.028 nats on balanced log-PPL ( $t= -4.46$ ,  $p=0.047$  in the primary attribution chain;  $t= -3.47$ ,  $p=0.074$  in the consistency chain). An auxiliary  $\alpha=0$  inheritance counterfactual at  $n=3$  seeds is sign-inconsistent at the headline metric (+3.18% on seed 42, -1.65% on seed 137, +0.20% on seed 256, mean +0.56%) and is underpowered for either a load-bearing or an equivalence conclusion on the inheritance sub-component (an earlier draft of this paper claimed the counterfactual ruled out inheritance under an arithmetic-mean aggregator; that claim is retracted, see Appendix B.11). A base-perturbation probe directionally refutes a “genomic-context” reframe of the lifecycle role (Section 7).
- **A substrate-conditional regime boundary.** On a controllable synthetic sandbox where ground truth is known, evolutionary search on the routing channel is load-bearing *only* when adapters are pre-aligned to the task; in every other regime tested (joint random initialization, gradient-warm initialization, hybrid ES-then-SGD) evolutionary search underperforms, ties, or actively degrades the gradient solution (Section 4). The production-substrate result is consistent with this boundary.

**Why (evidence).** The decomposition is not retrospective. We pre-specified a 5-of-8 partial  $2^3$  factorial over three factors — F1 router rewrite, F2 per-domain LOO evaluation scope, F3 lifecycle dynamics — and ran  $n=3$  seeds per cell at 25000 training steps each on the widened-1536 from-scratch substrate (15 production runs in the core factorial; 4 additional runs in the Fork 0 seed sweep). Numerical claims in this paper trace to source-of-truth analysis JSONs in `experiments/trackb_b2/analysis/`; per-cell run identifiers, per-seed PPLs, and a full re-derivation of the headline statistics from those JSONs are reproduced in Appendix A and Appendix D.

**So what (significance).** The most important finding is not that lifecycle dynamics fail, but *that they fail in a specific, characterizable way*: the system’s balanced-aggregate win on this substrate is carried by a structural routing fix, and the evolutionary machinery layered on top of that fix is mildly anti-aligned with the gradient solution that the routing fix unlocks. This is a sharper statement than “lifecycle did not help”; it is a statement about *when, on what substrate, and against what gradient signal* a particular evolutionary design might be expected to contribute. The synthetic-sandbox result in Section 4 provides a candidate sufficient condition for ES contribution (oracle-aligned adapters carrying informative routing signal). The production-substrate result is not in that regime. We make no claim that mixture-of-LoRA evolution *cannot* pay rent — only that the particular configuration we tested, on the particular substrate we tested it on, does not. We expect this paper to be most useful to readers who are about to spend compute on a similar evolutionary design and want a falsifiable prior on which sub-mechanisms are most likely to carry value.

**What the paper is not.** We are not claiming a state-of-the-art mixture-of-LoRA result; the absolute perplexity numbers are produced by a  $\sim 150\text{M}$ -parameter from-scratch base trained for 70000 steps on a

domain-mixed 32k-vocab corpus, and the 25000-step adaptation budget is small. We are not claiming the lifecycle penalty is universal; the budget, the inheritance schedule, the mutation rate, the lifecycle cadence, the specific kill gate, and the substrate width are all design choices that could be wrong. We are not claiming that the synthetic-sandbox oracle-alignment boundary transfers cleanly to all production mixture-of-LoRA setups — only that it transfers in the one direction we have measured (a substrate not in the oracle-alignment regime fails to benefit from ES, consistent with the boundary). The limitations (Section 8) are as central to the paper as the headline numbers.

**Roadmap.** Section 2 positions the work against mixture-of-experts, parameter-efficient adaptation, and the evolutionary-strategies-vs-gradient-descent literature. Section 3 describes the substrate, eval pipeline, and audit chain. Section 4 reports the synthetic-sandbox boundary result. Section 5 reports the production-substrate 5-cell partial factorial. Section 6 explains why the router rewrite carries the win. Section 7 reports the auxiliary ablations on the lifecycle penalty (Phase B and Fork 0). Section 8 states the limitations in the TMLR-conventional extensive form, and Section 9 lists the planned follow-ups, including the four-cell sub-factorial that would isolate the gate-function rewrite from the routing-input change inside F1, and the F3 sub-component decomposition that would isolate death and reproduction from inheritance and mutation.

## 2 Related work

We organize the related work methodologically rather than paper-by-paper, around the three factors that the production-substrate factorial decomposes (Section 5): the routing channel itself, the evolutionary lifecycle that operates on the adapter population, and the evaluation methodology that aggregates per-domain signals into a balanced headline.

**Routing in mixture-of-experts and mixture-of-LoRA.** The closest prior work to our F1 factor is the line on top- $k$  routed mixture-of-experts, in which a parameterized router selects a sparse subset of expert sub-networks per token and the un-selected experts are not computed (Fedus et al., 2021; Zoph et al., 2022). Two recurring pathologies have been reported in this line: (i) router collapse, in which a small subset of experts captures all of the routing mass and the others are routing-dead, addressed by load-balancing auxiliary losses and z-loss penalties (Zoph et al., 2022); and (ii) routing-input under-specification, in which the gate function does not have access to a representation rich enough to differentiate expert specialties, addressed by alternative routing schemes such as expert-choice (Zhou et al., 2022). Mixture-of-LoRA extensions of this line replace dense MLP experts with parameter-efficient LoRA adapters layered on a frozen backbone (Hu et al., 2021; Li et al., 2024). The coalition monopoly we measure on the legacy softmax router (Section 6.1) is in pathology family (i), and the routing-input change from token-embedding mean to post-stack hidden state is in pathology family (ii). Our F1 contribution is not in identifying these pathologies, which are known, but in *decomposing the production-substrate gain by attribution chain* and showing that the routing fix carries the entire balanced-PPL win on this substrate.

**Evolutionary search on neural-network parameters.** The evolutionary side of the system inherits from a long line of neuroevolution and population-based work. Evolution strategies (ES) have been studied as a scalable alternative to reinforcement learning on policy-network parameters (Salimans et al., 2017), and as a generic search method on neural architectures and weights (Stanley et al., 2019). Whether ES is best read as a finite-difference gradient estimator or as a fundamentally different search scheme has been studied directly (Lehman et al., 2018); the question is empirical, depends on the regime, and informs the synthetic-sandbox oracle-alignment boundary we report in Section 4. Population-based training of neural networks (Jaderberg et al., 2017) introduces a related but distinct mechanism: copying the weights of a fitter model into a less fit one and mutating its hyperparameters in place. Hardware-accelerated neuroevolution frameworks (Tang et al., 2022) make population methods tractable on modern accelerators. Our F3 contribution is not in introducing a new evolutionary primitive — death, reproduction with heritable mutation, and inheritance via  $\alpha$ -blend into a nearest neighbor are familiar pieces — but in measuring whether their *aggregate effect* on a particular adapter-evolution substrate is positive, null, or negative.

**Evolutionary methods on large language models.** A more directly competitive recent literature applies evolutionary search to large language models themselves rather than to small policy networks. Qiu et al. (2025) report that ES on full-parameter LLM fine-tuning is competitive with reinforcement learning at the scales tested; Sarkar et al. (2025) introduce a low-rank-structured ES variant (EGGROLL) targeting hyperscale; and Korotyshova et al. (2025) apply CMA-ES to LoRA singular values up to 72B parameters. Liang et al. (2026) give a variance-curvature account of why these low-rank evolutionary methods often outperform full-parameter search, which our synthetic-sandbox boundary (Section 4) reads as direction-aligning with the oracle-alignment requirement we measure. Feng et al. (2025) jointly optimize the roles and weights of multi-LLM systems via particle-swarm optimization. The Sakana line on evolutionary model-merging (Akiba et al., 2024; Kuroki et al., 2024; ao Abrantes et al., 2025) and the SVF/Transformer-Squared self-adaptation work of Sun et al. (2025) are closest in spirit to our F1 factor: the gains there come from a *structural* change to the adapter-combination machinery rather than from in-training population dynamics, which matches our finding that the routing rewrite carries the entire balanced-PPL win. Abdi et al. (2026) report that ES on LLM fine-tuning induces catastrophic forgetting, and Kumaresan (2026) provide a quantitative population-fusion model for cooperative LLM training. The lifecycle penalty we report is sign-consistent with the forgetting result of Abdi et al. (2026), although the substrate is mechanistically distinct (per-layer LoRA adapters under top- $k$  routing on a frozen base, vs. full-parameter ES on an unfrozen base). What the present paper adds over this literature is *factor isolation*: rather than reporting an aggregate full-system-vs-static contrast, we attribute the contrast to a router rewrite (load-bearing), a per-domain leave-one-out scope (null), and a lifecycle (net drag), which lets the paper speak both to “does evolutionary search on LLM adapters work” and to “which factor of the standard evolutionary-mixture-of-LoRA recipe carries the work.”

**Recycling, autophagy, and the cost of population dynamics.** A separate line of work studies what happens when generative models consume their own outputs across generations, finding that a model trained on data generated by an earlier generation of itself can suffer a “model autophagy disorder” in which diversity collapses and reconstruction fidelity degrades (Alemohammad et al., 2023). The lifecycle penalty we report is not autophagy in this sense (the base model is frozen and there is no generative-output feedback loop), but the analogy informs why inheritance — a mechanism that explicitly recycles a fraction of the dying adapter into the surviving population — might pay a cost rather than a benefit. The Fork 0 Phase A and Phase B ablations (Section 7.3, 7.1) test for this directly and locate the inheritance-versus-survival correlation as age-confounded rather than causal.

**Selection versus self-correction.** A complementary observation in the language-model literature is that LLMs frequently fail to self-correct their own reasoning when the correctness signal is internal rather than externally verified (Huang et al., 2024). The selection step in our lifecycle (a held-out leave-one-out fitness evaluation that decides which adapter dies) is in spirit a population-level external correctness signal, in contrast to a single-adapter self-correction loop. We do not take a position on whether population selection generally beats self-correction in the language-model setting, but we note that the *form* of the signal in our system — a per-adapter loss on a held-out micro-batch with forced single-adapter routing — is of the kind the self-correction-failure literature would expect to be load-bearing if anything is. The fact that this strong selection signal co-exists with a net lifecycle penalty (Section 5) is therefore informative: it suggests the penalty is not from a poor-quality fitness signal but from somewhere else in the F3 mechanism (mutation distribution, slot reallocation policy, lifecycle cadence; see Section 7.5).

**Multi-level optimization framing.** A recent line frames many learning systems as nested optimizers (Behrouz et al., 2025): a fast inner loop (here, SGD on adapter parameters) embedded inside a slower outer loop (here, the evolutionary lifecycle on the adapter population). On this framing, the lifecycle penalty we measure is a statement about the *coupling* between the two levels — specifically, that on this substrate, the outer-loop selection-and-mutation schedule is mildly anti-aligned with the inner-loop gradient flow, rather than a statement that two-level optimization is unhelpful in general.

**Reproducibility and verification methodology.** The verification protocol applied to this paper draws on the broader machine-learning reproducibility literature (Pineau et al., 2020; Henderson et al., 2018): every numerical claim in this paper carries a comment-level link to a single source-of-truth JSON or analysis

document, and Appendix B logs the corrections applied during paper preparation as a transparency artifact for readers who want to verify reproducibility against the supplement.

### 3 Infrastructure: substrate, evaluation, and source-of-truth conventions

This section describes the production substrate on which the real-text factorial of Section 5 runs, the evaluation pipeline that aggregates per-domain held-out signal into the balanced log-PPL headline, and the audit chain that anchors every numerical claim to a source-of-truth file. The synthetic sandbox of Section 4 runs on a separate, much smaller substrate documented at the top of that section.

#### 3.1 Substrate

The base model is a  $\sim 150\text{M}$ -parameter from-scratch GPT-style transformer with hidden size  $D=1536$ , 12 layers, 16 attention heads, sequence length 1024, vocabulary size  $V=32000$ . The  $D/V=1536/32000 \approx 0.048$  ratio is intentionally widened relative to the prior  $D=1024, V=32000$  ( $D/V \approx 0.032$ ) substrate, to reduce the gradient-norm-destruction effect at the LM head<sup>1</sup> and to give adapters more headroom to differentiate. The base is pre-trained for 70000 steps on a 32k-vocabulary domain-mixed corpus (`tokenized_mixed32k_b2`) covering biology, code, general text, and science domains. The frozen pre-train checkpoint `checkpoints/base_model_trackb_b2_dv1536/base_step_70000.pt` is the canonical base for all production-substrate experiments in this paper. We acknowledge in Section 8 that the base training was halted at step 70000 rather than at the originally planned step  $\sim 143000$  owing to a UPS power-event interruption; the ablations in this paper are therefore comparable against each other but not against the originally-planned, longer-trained base.

LoRA adapters are injected at every transformer block on the `query_key_value`, `dense`, `dense_h_to_4h`, and `dense_4h_to_h` projections, with rank  $r=8$  and  $\alpha=16$ . The static population size is  $P=16$  adapters; the sparse top- $k$  is  $k=4$ . Adapter-side optimization uses AdamW with learning rate  $10^{-4}$ ; the router uses a decoupled AdamW at  $10^{-5}$ . The adaptation horizon is 25000 steps for each cell of the factorial.

#### 3.2 Evaluation pipeline

The eval signal is held-out per-domain perplexity, computed on a balanced eval mixture across the four domains. The pipeline splits into two layers.

**Per-domain loaders.** Each of the four domains has its own evaluation `DataLoader` constructed from a pre-tokenized shard manifest (`shard_metadata.json`). Each shard carries an explicit domain tag mapped through a canonical-name alias table; shards whose domain tag is missing or unrecognized are excluded. The per-domain loaders draw from the held-out split (`eval`) of the pre-tokenized 32k-vocab corpus, use a fixed eval microbatch size of 32 sequences, and are deterministic given the configuration’s random seed.

**The StratifiedEvalLoader.** A pre-existing bug in the legacy `build_data_loader(split="eval")` path constructed a single concatenated eval loader by alphabetical shard ordering, with the consequence that the first batches drawn from the concatenated loader came entirely from the alphabetically-first domain shards (in the `tokenized_mixed32k_b2` layout, this is `biology`, since the four domain names ordered alphabetically are `biology < code < general < science` and the first concatenated shard is `shard_0000.npy` from the biology domain). Any  $N$ -batch eval consumer therefore saw an unbalanced mixture biased toward whichever domain appeared first in shard-name order. `StratifiedEvalLoader` (in `uyir/data_utils.py:271-318`) yields exactly one batch per domain per iteration cycle in alphabetical-domain-name order, with per-domain iterator state persisted across `__iter__` calls so that successive cycles progress through each domain’s data rather than replaying the first shard. The fix went in at git `6b00021`; all production runs in this paper use the

<sup>1</sup>An in-code comment in `uyir/training.py` attributes this design choice to internal experiments showing that wider  $D/V$  ratios produce adapter populations with measurably more cross-domain signal in routing inputs; the F1 routing-input change in Section 6.3 relies on the same effect.

post-fix stratified eval loader. We list the deflation-of-cross-seed-variance side-effect of this fix as a limitation in Section 8.

**Headline aggregator.** We use the *geometric mean* across domains as the headline balanced-PPL aggregator:  $\text{PPL}_{\text{balanced}} = \exp(\frac{1}{4} \sum_d \log \text{PPL}_d)$  over  $d \in \{\text{biology, code, general, science}\}$ . This convention is pinned in Section 5.1. The geometric mean is the appropriate aggregator for log-PPL paired tests because  $\Delta \log \text{PPL}_{\text{balanced}}$  then equals the mean of per-domain  $\Delta \log \text{PPL}_d$ , which is the additive quantity the per-seed paired- $t$  tests in Section 5 act on. An arithmetic mean of per-domain PPLs (used by some prior reports including an earlier internal Phase B summary) does not have this additive property and is not used as the headline in this paper.

**Two evaluation scopes.** Factor F2 in Section 5 contrasts two scopes: *aggregate-LOO*, in which the four per-domain loaders are flattened to a single uniform-mixed eval batch and a single LOO fitness signal is computed against that aggregate; and *per-domain-LOO*, in which each adapter is evaluated against its own per-domain held-out batch and the per-domain LOO scores are averaged. The factorial measures whether the choice of scope on its own contributes to the balanced-PPL win; the answer (Section 5) is null at seed-resolution.

### 3.3 Source-of-truth conventions

Numerical claims in this paper trace to single source-of-truth files in `experiments/trackb_b2/analysis/`, with a corresponding `% source: <path>:<key>` comment in the LaTeX immediately adjacent to the cited number. We follow three conventions for self-consistency. First, citations resolve to underlying analysis JSONs or per-run outputs rather than to rolled-up summary files (`RESULTS.md`, `STATUS.md`, project notes), which can drift from the JSON they were meant to summarize. Second, sign convention, aggregator, and degrees-of-freedom are pinned at section entry rather than left implicit; Section 5.1 pins “improvement-is-positive” on log-PPL with  $\Delta = \log \text{PPL}_{\text{ref}} - \log \text{PPL}_{\text{test}}$  and the geometric-mean aggregator. Third, headline statistics are re-derived from per-seed JSON: the headline full-system-vs-B3 balanced contrast at  $n=3$  is paired- $t$   $t=1.94$ ,  $p=0.19$ ,  $df=2$ , and the code-domain single-cell paired- $t$  is  $t=10.42$ ,  $p=0.009$ ,  $df=2$  (full re-derivation in Appendix D). Corrections applied to draft text during paper preparation are logged in Appendix B as a transparency artifact.

### 3.4 Reproducibility footprint

The full hyperparameter inventory, per-cell W&B run identifiers, and configuration JSONs for all 19 production runs (15 in the core factorial, 4 in the Fork 0 seed sweep) are in Appendix A. The synthetic-sandbox per-seed numbers (Appendix C) and the corrections log (Appendix B) are intentionally extensive in keeping with TMLR’s emphasis on extensive reproducibility documentation.

## 4 Synthetic boundary characterization (G4–G8)

Before measuring whether evolutionary search adds value to a real mixture-of-LoRA training pipeline, we ask whether evolutionary search adds value *anywhere* on a controllable substrate where ground truth is known. This section describes a five-experiment battery (G4–G8) on a purpose-built synthetic sandbox. The battery defines a regime boundary: evolutionary strategies (ES) are load-bearing on the routing channel *only* when adapters are pre-aligned to the task; in every other regime tested (joint random initialization, gradient-warm initialization, hybrid ES-then-SGD schedules) ES underperforms, equates, or actively degrades the gradient solution. Section 5 inherits this boundary as the prior expectation against which the real-text factorial is interpreted.

The full per-seed numbers and trajectories for each sweep are in Appendix C; this section reports cross-seed means with the relevant test statistic for each comparison.

## 4.1 Sandbox design

The sandbox is intentionally minimal so that any signal observed must come from the routing-and-adapter machinery rather than from data structure that could be solved by the base model alone. Vocabulary size is 128, partitioned into four disjoint slabs of 32 tokens each. Each slab indexes a single synthetic “domain.” Within a domain, the next token is a deterministic permutation of the current token, restricted to that slab; the resulting task is therefore a per-domain bigram prediction problem with a 32-way within-slab branching factor and a perfect achievable per-token loss of  $\log(1) = 0$  given correct routing.<sup>2</sup> Wrong-domain routing degrades to uniform over a slab, yielding  $\log(32) \approx 3.47$  nats. Random routing across all four slabs degrades further to  $\log(128) \approx 4.852$  nats. The substrate is a small frozen base model (hidden dimension 512), with  $K=16$  LoRA adapters and top- $k=4$  routing per token.

This dimensioning gives three reference loss values on every sweep: **oracle** (perfectly routed, perfectly specialised adapters,  $\approx 0.042$  nats), **random-router** ( $\approx 0.089$  nats), and **uniform** (4.852 nats).<sup>3</sup>

## 4.2 G4: oracle adapters, ES on the router (PASS)

The first experiment establishes that the routing channel is real and that ES can find it given a pre-aligned substrate. The protocol is three-phase: **(A)** oracle-routed pretrain for 3000 steps with adapter learning rate  $3 \times 10^{-3}$ ; domain  $d$  is forced to adapters  $[d \cdot k, (d+1) \cdot k)$  with the router bypassed, so each adapter mechanically specialises on a single domain. **(B)** snapshot, freeze the base and adapters, reset the router from  $\mathcal{N}(0, 0.02)$ . **(C)** 1500 steps of router-only training under each strategy. The strategies compared are SGD on the router (with router learning rates in  $\{10^{-4}, 10^{-2}\}$ , both returning the same outcome) and ES with antithetic mirror-pair noise at  $\sigma \in \{0, 10^{-3}, 10^{-2}, 10^{-1}, 1\}$ , three seeds each. The ES algorithm at every sigma uses 16 antithetic mirror pairs per step (i.e. 32 candidate evaluations per step), Gaussian perturbations  $\epsilon \sim \mathcal{N}(0, \sigma^2 I)$  applied additively/symmetrically to a flat parameter vector, and rank-based NES utility shaping. The update at each step is  $\theta \leftarrow \theta + (\eta/\sigma) \cdot (1/P) \sum_{i=1}^P u_i \epsilon_i$  with  $P=16$  pairs, outer learning rate  $\eta=1.0$ , and utilities  $u_i \propto \max(0, \log(P/2+1) - \log(i+1))$  normalised to unit  $L_1$  norm and mean-centred to give zero update under uniform fitness (reference implementation in `experiments/phase05_es_router/es_router.py`). The same algorithm and hyperparameters are used for the coupled-ES experiments in G5–G8; only the dimensionality of  $\theta$  changes (router-only in G4, router-plus-adapters in G5–G8).

Cross-seed means in Phase C are summarised in Table 1. SGD on the router closes **0.2 %** of the routing gap (oracle – random-router); ES at  $\sigma=0$  (provable no-op control) closes  $-0.1 \%$ , confirming that the ES infrastructure itself is not contaminating the comparison; ES at  $\sigma=10^{-1}$  closes **55.9 %** of the gap, with  $\sigma=10^{-3}$  at 17.4%,  $\sigma=10^{-2}$  at 26.2%, and  $\sigma=1$  at 45.5%. The  $\sigma$ -curve is monotone up to  $\sigma=10^{-1}$  and then degrades slightly at  $\sigma=1$  (excess exploration noise), the textbook signature of a meaningful ES signal.

The result is interpretable: with adapter–domain alignment baked in by oracle pretraining, the router needs only to rediscover a pre-existing mapping. The mapping is discoverable by black-box random search at  $\sigma=10^{-1}$  and not discoverable by SGD at any router learning rate we tested. The gap between the two strategies,  $0.0892 - 0.0629 = 0.026$  nats, exceeds three SGD seed standard deviations ( $3 \cdot 0.0014 = 0.0042$ ) by more than a factor of six. We label this regime **ES PASS**.

The mechanism is the non-differentiability of `torch.topk`. Given a sparse top- $k$  selection, the gradient signal arriving at the router logits is restricted to the  $k$  already-selected entries; an unselected entry receives no information about whether selecting it would have improved the loss. With oracle adapters and a small selection ( $k=4$  of  $K=16$ ), the unselected entries dominate the search space, and SGD has no way to explore them. ES at  $\sigma=10^{-1}$  explores the selection itself: mirror-pair antithetic perturbations of the router parameters change which adapters are selected, and the rank-shaped utility update integrates information

<sup>2</sup>In practice the sweep code mixes the deterministic bigram with a small uniform smoothing, so the oracle endpoint is  $\approx 0.042$  nats rather than zero. See `experiments/phase05_es_router/synth_data.py` for exact distributions.

<sup>3</sup>The random-router floor sits much closer to oracle than to uniform because the oracle-pretrain of Phase A bakes the per-domain mapping into the adapters: with  $K=16$  adapters specialised four-per-slab and top- $k=4$  selection from  $\mathcal{N}(0, 0.02)$  router logits, the soft mass over the four correct adapters is on average sufficient to recover most of the within-slab signal even before any router learning. The oracle vs. random-router gap ( $\approx 0.047$  nats) is therefore the headroom that ES is asked to close in G4, not the full 4.852 nats uniform-vs-oracle spread.

Table 1: G4 positive control: ES on the router, oracle-aligned adapters frozen. Cross-seed mean ( $n=3$ ) of Phase-C val loss; gap-closed is the fraction of the oracle-random-router gap recovered. Best ES ( $\sigma=10^{-1}$ ) closes 55.9% of the gap; SGD closes 0.2%. The SGD-on-router and random-router rows both round to 0.0892 at the fourth decimal place; the 0.2% gap-closed for SGD is computed from the unrounded cross-seed mean (full-precision values in the `positive_control_results.json` source-of-truth file).

mode	$\sigma$	mean val loss	std	gap closed
oracle (lower bound)	—	0.0422	—	100%
random-router (upper bound)	—	0.0892	—	0%
SGD on router	—	0.0892	0.0014	0.2%
ES	0	0.0893	0.0010	-0.1%
ES	$10^{-3}$	0.0811	0.0022	17.4%
ES	$10^{-2}$	0.0769	0.0026	26.2%
ES	$10^{-1}$	<b>0.0629</b>	0.0037	<b>55.9%</b>
ES	1	0.0678	0.0025	45.5%

from all selections within the perturbation pair, including ones that are unreachable by gradient. This is the only regime in G4–G8 where that channel is load-bearing.

### 4.3 G5: random initialization, joint coupled ES (small effect, near uniform)

Removing the oracle pretrain weakens the result substantially. In G5, the base is frozen and ES drives the router *and* the adapters jointly via a single flat parameter vector of  $\sim 557,000$  dimensions. There is no Phase A; the adapters are random LoRA initializations. We compare joint coupled-ES against SGD-all (frozen base, SGD on router and adapters jointly), 1500 steps each. The 3-seed initial sweep was borderline; we re-ran with  $n=10$  seeds to settle the question.

Cross-seed means  $\pm$  sample standard deviation are: SGD-all  $4.898 \pm 0.032$  nats; coupled-ES at  $\sigma=10^{-3}$ ,  $4.835 \pm 0.054$  nats; coupled-ES at  $\sigma=10^{-1}$ ,  $4.864 \pm 0.019$  nats.<sup>4</sup> The Welch test below uses these as the per-arm sample standard deviations with  $n=10$  seeds, giving per-arm SEMs of 0.010, 0.017, and 0.006 respectively. A two-sample Welch test on the  $\sigma=10^{-3}$  effect gives  $t = -3.16$  ( $df \approx 15$ ,  $p = 0.0067$ ); on the  $\sigma=10^{-1}$  effect,  $t = -2.85$  ( $df \approx 14$ ,  $p = 0.012$ ). Both are statistically distinguishable from SGD-all under a coherent two-sample test, and we therefore do not call this regime ambiguous.

The substantive caveat is that the absolute values are at or just below the uniform-prediction floor. Best coupled-ES ( $\sigma=10^{-3}$ , 4.835 nats) sits one standard error of the mean below uniform ( $0.054/\sqrt{10} = 0.017$ ); SGD-all sits one standard error *above* uniform. ES descends faster from random adapters than SGD does on the same compute, but it descends from  $\approx 5.0$  nats to  $\approx 4.83$  nats over 1500 steps, whereas the same substrate under oracle adapters reached 0.063 nats. The G4 ES PASS is not generic “ES exceeds SGD”; it is “ES finds routing if adapters are pre-aligned.” G5 confirms this reading: with random adapters, ES is paired-test distinguishable from SGD but neither strategy makes meaningful progress in the available budget. These G5 cross-seed means are reported in prose only; Table 2 below reports the G6 warm-start sweep, not G5.

### 4.4 G6: gradient-warm prior, ES tail (warm-start INERT)

If the G5 result is bottlenecked by adapter randomness, a non-oracle but non-random prior should help. G6 tests this. Phase A is 5000 steps of SGD on (router + adapters) from random initialization, no oracle, on the same frozen base. The Phase-A endpoint is  $4.549 \pm 0.047$  nats, substantially below uniform. Phase B then runs each strategy for 1500 more steps from this checkpoint.

The cross-seed Phase-B endpoint and warm-start delta  $\Delta_{\text{warm}} = (\text{val}_B) - (\text{warmup val})$ , with positive  $\Delta_{\text{warm}}$  meaning the loss *regressed* from the warm prior, are reported in Table 2. SGD-continue descends 0.180 nats

<sup>4</sup>Uniform on a 128-token vocabulary is  $\log(128) = 4.852$  nats.

Table 2: G6 warm-start coupled-ES sweep. Cross-seed mean ( $n=3$ ) of Phase-B val loss starting from a 5000-step SGD warm prior at  $4.549 \pm 0.047$  nats.  $\Delta_{\text{warm}}$  is positive when ES regresses the prior. SGD-continue descends a further 0.18 nats; every nonzero ES  $\sigma$  regresses by 0.27 nats or more.

mode	$\sigma$	Phase-B mean	std	$\Delta_{\text{warm}}$
SGD-continue	—	4.369	0.055	-0.180
ES (control)	0	4.540	0.049	-0.009
ES	$10^{-3}$	4.815	0.042	+0.265
ES	$10^{-2}$	5.005	0.056	+0.456
ES	$10^{-1}$	4.837	0.034	+0.288
ES	1	4.967	0.023	+0.417

below the warm prior; every ES sigma we tested (**including the no-op control  $\sigma=0$  and four orders of magnitude of nonzero  $\sigma$  in G7 below**) regresses the warm prior.

We label this regime **warm-start INERT**. The sign convention used here is  $\Delta_{\text{warm}} = \text{val}_B - \text{warmup}$ , with positive values meaning regression above the warm baseline; this convention matches the source-of-truth analysis JSON for the warm-start small-sigma sweep (`warmstart_smallsigma_results.json`).

#### 4.5 G7: small- $\sigma$ refutation of the sigma-matching hypothesis

A natural objection to G6 is that the tested sigmas were too large: ES might require  $\sigma$  matched to substrate sharpness, and the warm prior might be preserved at  $\sigma \ll 10^{-3}$ . G7 tests this directly with  $\sigma \in \{10^{-5}, 10^{-4}, 5 \times 10^{-4}, 10^{-3}\}$  across five seeds.

The result refutes the sigma-matching story with the strongest possible evidence: not only do small sigmas regress the warm prior, *they regress it more*. Cross-seed mean  $\Delta_{\text{warm}}$  in nats:  $+0.4673$  at  $\sigma=10^{-5}$ ;  $+0.4583$  at  $\sigma=10^{-4}$ ;  $+0.3557$  at  $\sigma=5 \times 10^{-4}$ ;  $+0.2378$  at  $\sigma=10^{-3}$ . The trend is monotone in the wrong direction: smaller  $\sigma$  yields larger regression. SGD-continue, by comparison, descends  $\Delta_{\text{warm}} = -0.1772$  over the same horizon.

A sigma-matching mechanism would predict a U-shape in  $\Delta_{\text{warm}}$  versus  $\sigma$ , with some sigma preserving the prior. The observed monotone-wrong-direction shape rules out sigma-matching as the explanation. The most parsimonious reading is that the rank-shaped utility update at small  $\sigma$  drives the population off the SGD-found basin without enough exploitation gradient to relocate to a comparable basin within 1500 steps; smaller  $\sigma$  produces less exploitation per step and therefore wanders further. This reading is consistent with G6 and with G8 below.

#### 4.6 G8: hybrid ES-then-SGD (HARMFUL)

The remaining open ES design point is whether ES early-stage exploration can find a basin that SGD can subsequently exploit better than pure SGD descent from random initialization. G8 tests this. Both arms run a matched 6500-step compute budget. `pure_sgd` runs 6500 steps of SGD-all from random initialization. `es_then_sgd` runs 5000 steps of coupled-ES at  $\sigma=10^{-3}$  (the best single sigma from G5) followed by 1500 steps of SGD-all on the resulting state. A third arm, `pure_es`, runs 6500 steps of coupled-ES at the same sigma.

Cross-seed means ( $n=5$ ): `pure_sgd`  $4.386 \pm 0.053$  nats; `es_then_sgd`  $4.693 \pm 0.040$  nats; `pure_es`  $4.696 \pm 0.054$  nats. Pure SGD beats hybrid by 0.307 nats, which is  $6 \times$  the SGD seed standard deviation.

The SGD-tail recovery from the ES-warm prior is small but nonzero. The correct paired statistic is the cross-seed mean of per-seed (`phase_a` – final), where `phase_a` is each seed’s ES-warmup endpoint val loss after 5000 steps of  $\sigma=10^{-3}$  ES. Computed correctly across all five seeds, this paired difference is  $+0.0203$  nats (paired  $t=1.65$ ,  $df=4$ ,  $p > 0.05$ , not significant at  $\alpha=0.05$ ).

For context, equal-budget pure SGD descends  $4.852 - 4.386 = 0.466$  nats from the uniform-prediction floor in 6500 steps; the SGD tail from an ES-warm prior descends 0.020 nats. The ratio is approximately  $16 \times$ .

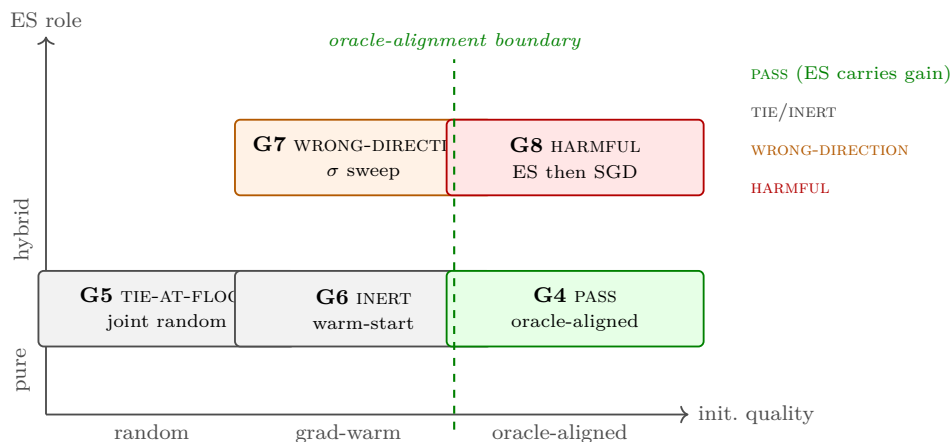


Figure 1: Synthetic-sandbox regime map. ES is load-bearing on the routing channel only inside the oracle-alignment regime (G4): adapters pre-aligned to the per-slab oracle plus small noise, ES at  $\sigma=10^{-1}$ , closes  $\approx 55.9\%$  of the routing-loss gap while the SGD contrast closes  $\approx 0.2\%$ . Outside the boundary, ES is inert (G5/G6), regresses monotonically with  $\sigma$  (G7), or is strictly harmful in the hybrid setting (G8). The headline production- substrate result in Section 5 is consistent with the production substrate being on the wrong side of this boundary.

The 1500 SGD steps after ES recovered roughly 5% of what 6500 steps of pure SGD achieves at matched compute. Concretely, `es_then_sgd` (4.693 nats) is statistically indistinguishable from `pure_es` (4.696 nats): the SGD tail extracts a small amount of descent (0.020 nats) from the ES-warm prior, but it is small enough that the ES warmup essentially determines the final outcome. We label this regime **hybrid HARMFUL**.

#### 4.7 Boundary characterization synthesis

Across G4–G8, the regime structure is:

- **G4 (oracle adapters, ES on router): PASS.** ES at  $\sigma=10^{-1}$  closes 55.9% of the routing gap; SGD closes 0.2%.
- **G5 (random init, coupled ES): SMALL EFFECT, NEAR UNIFORM.** ES paired-test distinguishable from SGD-all ( $\sigma=10^{-3}$ ,  $t=-3.16$ ,  $p=0.0067$ ,  $n=10$ ); both strategies stay near uniform at 1500 steps.
- **G6 (SGD warm + ES tail): INERT.** Every nonzero  $\sigma$  regresses the warm prior by 0.27 nats to 0.46 nats; SGD-continue descends 0.18 nats.
- **G7 (SGD warm + small  $\sigma$ ): INERT, monotone wrong direction.**  $\sigma=10^{-5}$  yields  $\Delta_{\text{warm}} = +0.467$ ; sigma-matching hypothesis refuted.
- **G8 (ES warm + SGD tail): HARMFUL.** Pure SGD beats ES-then-SGD by 0.31 nats ( $6\times$  SGD seed std); SGD tail from ES-warm recovers 0.020 nats,  $16\times$  less than equal-budget pure SGD.

The unified reading is that ES is load-bearing on this substrate *exclusively* in the regime where the routing channel exists as a non-differentiable selection over a set of pre-aligned options. G4 satisfies that condition. None of G5–G8 satisfies it. We will refer to this as the *oracle-alignment boundary* for the remainder of the paper.

The substantive consequence for the real-text mixture-of-LoRA setting is a prior expectation: the lifecycle mechanism (death, inheritance, mutation, reallocation) operates on adapters that are simultaneously being trained by gradient. There is no oracle pretrain; adapters are co-evolving with the router under the next-token loss gradient flowing through the frozen base, on a non-stationary stream of training tokens (the base

parameters themselves do not receive gradient updates). The G4–G8 boundary predicts that any evolutionary mechanism acting on this regime should resemble G5–G8 outcomes (small effect, inert, or harmful) more than it resembles G4. Section 5 reports the empirical test of that prediction on the production substrate.

## 5 Real-text decomposition: a 5-cell partial $2^3$ factorial

Section 4 established that on a controllable sandbox, evolutionary search is load-bearing only inside an oracle-alignment regime, and inert, harmful, or wrong-direction in every other regime tested (G5–G8). **The production substrate is not in the oracle-alignment regime:** there is no oracle pretrain; adapters are randomly initialised at the start of adaptation; the routing channel and the adapter weights co-evolve under the same next-token gradient. The synthetic boundary therefore predicts, before any production-substrate measurement is consulted, that the evolutionary machinery on the production substrate should resemble the G5–G8 outcomes (small effect, inert, or harmful) more than the G4 outcome. This section reports the empirical test of that prediction. We now ask whether the analogous evolutionary machinery on the production substrate, where adapters are co-evolving with the router under the gradient signal of the next-token loss flowing through a frozen base on a non-stationary text mixture (the base parameters do not receive updates), produces a different verdict. This section reports a 5-cell partial  $2^3$  factorial with three seeds per cell ( $n=15$  runs total) that decomposes the headline full-system-versus-B3 outcome into three mechanistic factors and isolates which of them carries the win.

The headline finding is that the router rewrite carries the entire balanced mixture-of-LoRA improvement; the per-domain LOO evaluation scope contributes nothing within seed-resolution; and the lifecycle mechanism (death, inheritance, mutation, reallocation) is a net drag of approximately 0.028 nats on balanced log-PPL ( $p=0.047$  in the primary chain,  $p=0.074$  in the consistency chain). The headline full-system-versus-B3 balanced delta itself (+0.015 nats,  $t=1.94$ ,  $p=0.19$ ) is not significant at  $\alpha=0.05$  with  $n=3$  seeds; the only individually significant total is on the code domain. Section 6 analyses the mechanism behind the router-rewrite contribution; Section 7 reports the auxiliary Phase B and Fork 0 experiments that test alternative explanations for the lifecycle penalty.

### 5.1 Convention pin

All paired-test deltas in this section follow the convention  $\Delta = \log(\text{PPL}_{\text{reference}}) - \log(\text{PPL}_{\text{test}})$ , so that *positive*  $\Delta$  means the test cell improves over the reference cell. This is the “improvement-is-positive” convention on log-PPL. Balanced PPL is the geometric mean across the four eval domains {biology, code, general, science}, i.e.  $\exp(\frac{1}{4} \sum_d \log \text{PPL}_d)$ . Per-seed paired  $t$ -statistics are reported with  $df = n_{\text{seeds}} - 1$ .

### 5.2 Cell design and the 5-of-8 partial factorial

The full evolutionary system over the B3 baseline differs in three factors. **(F1) Router rewrite:** the production B3 router is replaced by a rewritten variant carrying a sigmoid floor and a last-hidden-state input gate, denoted “sigfloor + last\_hidden.” **(F2) Per-domain evaluation scope:** the evaluation aggregator switches from aggregate-LOO (uniform per-token mixing across an undifferentiated balanced eval) to per-domain LOO (separate per-domain dataloaders, geom-mean aggregated). **(F3) Lifecycle:** the population dynamics of death,  $\alpha$ -blend inheritance, SVD mutation, and slot reallocation are switched on, with  $\alpha=0.2$  blend strength and  $\sigma=0.01$  initial mutation rate in C4.

The full  $2^3$  factorial would require eight cells. We run five of the eight, chosen to support two attribution chains that converge through C4. A full  $2^3$  design would guarantee orthogonality of main-effect contrasts; a 5-of-8 partial does not, and main effects in our decomposition are partially confounded with two-factor interactions. The dual-chain consistency check (Section 5.5) bounds the magnitude of those interactions empirically rather than eliminating them by design.

The *primary chain* is  $C1 \rightarrow C2 \rightarrow C5 \rightarrow C4$ , which moves through factor space one factor at a time: F3 alone ( $C1 \rightarrow C2$ ), then F2 given F3 ( $C2 \rightarrow C5$ ), then F1 given F2 and F3 ( $C5 \rightarrow C4$ ). The *consistency chain* is  $C1 \rightarrow C3 \rightarrow C4$ , which combines F1+F2 in one step ( $C1 \rightarrow C3$ ) and then layers F3 on top ( $C3 \rightarrow C4$ ). The two

Table 3: 5-of-8 partial  $2^3$  factorial. Each cell is run with seeds  $\{42, 137, 256\}$  ( $n=3$ ) for 25 000 steps on the widened-1536 substrate.

cell	router rewrite (F1)	per-dom scope (F2)	lifecycle (F3)	role
C1	B3	aggregate	off	B3 baseline (anchor)
C2	B3	aggregate	on	isolates F3 alone
C5	B3	per-dom	on	isolates F2 given F3 on
C3	rewrite	per-dom	off	combined F1+F2 without F3
C4	rewrite	per-dom	on	full evolutionary system ( $\alpha=0.2$ )

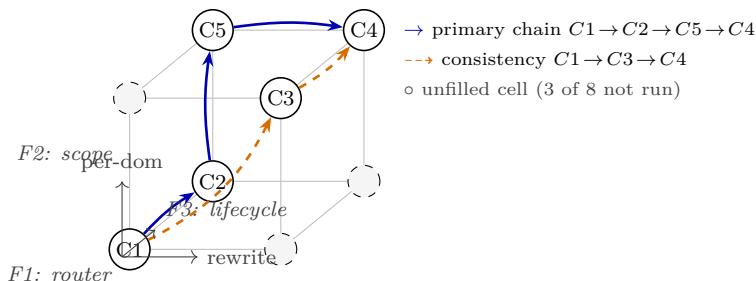


Figure 2: The 5-of-8 partial  $2^3$  factorial. Each filled corner is a cell we ran at  $n=3$  seeds; each unfilled corner is a cell we did not run. Two attribution chains start at the B3 baseline C1 and end at the full evolutionary system C4: the **primary chain** (solid blue) traverses one factor at a time ( $C1 \rightarrow C2$  adds F3 lifecycle,  $C2 \rightarrow C5$  adds F2 per-domain scope,  $C5 \rightarrow C4$  adds F1 router rewrite); the **consistency chain** (dashed orange) combines F1+F2 in one step ( $C1 \rightarrow C3$ ) and then layers F3 ( $C3 \rightarrow C4$ ). The two chains converge to within  $\sim 0.0004$  nats on each factor’s contribution (Section 5.6).

chains both start at C1 and end at C4. Their intermediate totals must agree on the aggregate F1+F2+F3 effect by additive identity in log-PPL, which provides a within-experiment consistency check on each factor’s estimated contribution.<sup>5</sup>

### 5.3 Per-cell balanced PPL

Table 4 reports the balanced PPL for each of the fifteen runs. The balanced PPL spread across cells is small in absolute terms ( $\sim 0.6$  PPL between best and worst cell means), reflecting that all cells share the same widened-1536 frozen base and only differ in the three factors above. Within-cell cross-seed variance is correspondingly small; the StratifiedEvalLoader is deterministic given seed, so several cell-seed pairs are bit-identical to other pairs at the per-domain PPL level (visible in the manifest in Appendix A, e.g.  $C5_{42}$  and  $C2_{42}$  co-incide on three of four per-domain values;  $C5_{137}$  and  $C5_{256}$  co-incide on all four). This deterministic eval pipeline deflates within-cell variance below what an i.i.d. resampling reading would predict, and we discuss the consequences for paired- $t$  inference in Section 8.

Two qualitative observations precede the formal attribution. First, C1 (B3 base) is tighter across seeds than any other cell: the seed-42 to seed-256 spread on C1 is 0.026 PPL versus 0.371 on C4. The B3 baseline is the most cross-seed-robust cell in this design; the C4 cell exhibits the widest cross-seed dispersion. Second, C3 outperforms both C4 and C1 on seed 42 and seed 256, and matches C4 closely on seed 137. The lifecycle mechanism, when added on top of the routing rewrite ( $C3 \rightarrow C4$ ), pushes PPL up rather than down on every seed.

<sup>5</sup>The omitted three cells are  $\overline{F1}F2F3$ —already in the design (this is C2);  $\overline{F1}\overline{F2}F3$  (B3 router, per-domain scope, lifecycle off);  $F1\overline{F2}F3$  (router rewrite, aggregate scope, lifecycle off);  $F1F2\overline{F3}$  (router rewrite, aggregate scope, lifecycle on). The two chains used here pin every factor’s contribution at least once and check the F1+F2 combined contribution twice (once via  $C5 \rightarrow C4$  router-only, once via  $C1 \rightarrow C3$  router+scope). A fully crossed  $2^3$  design at three seeds per cell would have cost a further three cells  $\times$  three seeds at the production budget; we chose breadth across the system’s other open experiments (Section 7) over factorial completion.

Table 4: Balanced PPL by cell and seed,  $\exp(\frac{1}{4} \sum_d \log \text{PPL}_d)$  over {biology, code, general, science}. Seed 42 was the original headline run; seeds 137 and 256 are the audit-driven cross-seed extension.

cell	seed 42	seed 137	seed 256
C1 (B3 base)	13.328	13.341	13.354
C2 (B3 + lifecycle)	13.538	13.805	13.832
C5 (B3 + per-dom + lifecycle)	13.564	13.778	13.805
C3 (rewrite + per-dom, no lifecycle)	12.742	12.830	12.742
C4 (full evolutionary system, $\alpha=0.2$ )	12.943	13.173	13.315

Table 5: Primary attribution chain on balanced log-PPL.  $\Delta = \log \text{PPL}_{\text{reference}} - \log \text{PPL}_{\text{test}}$ ; positive means improvement. Paired  $t$  across  $n=3$  seeds,  $df=2$ .

step	factor introduced	mean $\Delta$ (nats)	$t$	$p$
$C2 - C1$	lifecycle alone (B3 router, aggregate scope)	-0.0283	-4.46	0.047
$C5 - C2$	per-domain LOO scope (lifecycle on)	+0.0007	0.50	0.67
$C4 - C5$	router rewrite (sigfloor + last_hidden)	+0.0426	12.86	0.006

#### 5.4 Primary attribution chain $C1 \rightarrow C2 \rightarrow C5 \rightarrow C4$

Walking the primary chain one factor at a time gives the per-factor paired- $t$  statistics in Table 5. Each row is a paired test on the per-seed log-PPL difference between the two cells ( $df=2$ ).

The signs are unambiguous and consistent across seeds. **Lifecycle hurts:** adding the lifecycle on top of the B3 router and aggregate-LOO scope worsens balanced log-PPL by 0.028 nats on average across the three seeds, and the effect is significant at the  $\alpha=0.05$  level. **Per-domain LOO scope is null:** given lifecycle on, switching the eval aggregator from aggregate-LOO to per-domain LOO moves balanced log-PPL by less than 0.001 nats on average and the sign is inconsistent across seeds (positive on seeds 137 and 256, negative on seed 42). **Router rewrite carries:** given lifecycle on and per-domain scope, the router rewrite improves balanced log-PPL by 0.043 nats on average,  $t=12.86$ ,  $p=0.006$ .

#### 5.5 Consistency chain $C1 \rightarrow C3 \rightarrow C4$

The consistency chain combines F1 and F2 in a single step ( $C1 \rightarrow C3$ , no lifecycle) and then adds F3 on top ( $C3 \rightarrow C4$ , lifecycle on full). The chain estimates appear in Table 6.

The two chains agree to within a thousandth of a nat. The combined router+scope effect estimated as  $C3 - C1$  is +0.0436, while the same quantity decomposed via the primary chain as  $(C5 - C2) + (C4 - C5) = +0.0007 + 0.0426 = +0.0433$ ; the two estimates agree to 0.0003 nats. The lifecycle effect estimated as  $C4 - C3$  is -0.0287, while the primary-chain estimate  $C2 - C1 = -0.0283$  agrees to 0.0004 nats. The lifecycle effect remains negative in both chains; its  $p$ -value rises from 0.047 in the primary chain to 0.074 in the consistency chain (the effect is estimated against a different reference cell with slightly higher per-seed variance), but the sign and magnitude are stable. The dual-chain agreement acts as an internal consistency check that partially compensates for the incomplete 5-of-8 factorial: each factor’s contribution is estimated twice from non-overlapping cell pairs, and agreement across the two estimates bounds the magnitude of two-factor interactions empirically rather than eliminating them by design.

#### 5.6 Two-chain convergence and fractional attribution

The total balanced delta from  $C1 \rightarrow C4$  across all three factors is +0.0150 nats (paired  $t=1.94$ ,  $df=2$ ,  $p=0.19$ ). The total is not significant at  $\alpha=0.05$  with three seeds. The same total decomposes additively in log-PPL space along either chain:

Table 6: Consistency attribution chain on balanced log-PPL. Same convention and notation as Table 5.

step	factor introduced	mean $\Delta$ (nats)	$t$	$p$
$C3 - C1$	router rewrite + per-dom scope, no lifecycle	+0.0436	18.58	0.003
$C4 - C3$	lifecycle on top of full router + scope	-0.0287	-3.47	0.074

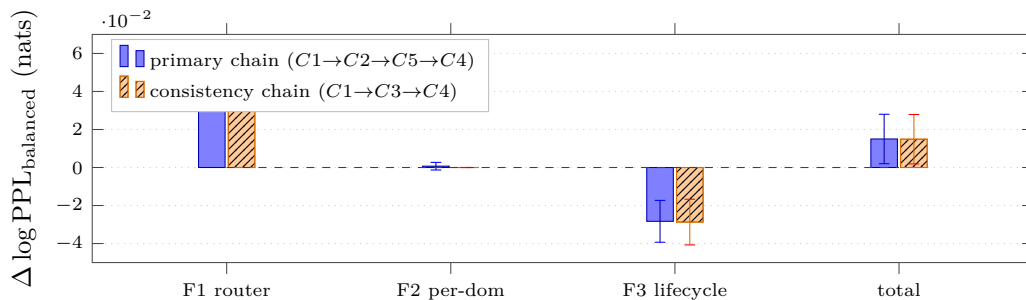


Figure 3: Per-factor balanced-log-PPL attribution, in nats. Bars are mean across  $n=3$  seeds; whiskers are the per-seed paired- $t$  standard error ( $df=2$ ). Primary chain (solid blue) decomposes factor-by-factor; consistency chain (orange, hatched) combines F1+F2 in one step (the F2-only bar in the consistency chain is therefore zero-by-construction). The two chains agree to within  $\sim 0.0004$  nats on each factor. F1 router rewrite carries the entire balanced full-system-vs-B3 improvement; F2 per-domain LOO scope is null at seed-resolution; F3 lifecycle is a net drag of  $\sim 0.028$  nats. The total  $C4 - C1$  is  $+0.015$  nats,  $t=1.94$ ,  $p=0.19$  at  $n=3$ , and does not clear  $\alpha=0.05$ .

$$\begin{aligned} \text{primary:} & \quad -0.0283 + 0.0007 + 0.0426 = +0.0150 \\ \text{consistency:} & \quad +0.0436 + (-0.0287) = +0.0149. \end{aligned}$$

The fractional attribution  $\Delta_{\text{factor}}/\Delta_{\text{total}}$  is mathematically defined and listed in Table 7 for completeness, but we caution against citing it without the small-total caveat: the total is approximately one-third of either single-factor effect, and the ratios diverge to large absolute values for individual seeds where the total approaches zero. For seed 256 the total  $\Delta = +0.003$  and the fractional decomposition is roughly  $-12 + 0.7 + 12 = 1$ , mathematically exact and substantively misleading.

The mean-across-seeds row in Table 7 reads as “router rewrite contributes roughly six times the total improvement; lifecycle subtracts roughly five times the total improvement; per-domain scope contributes roughly a quarter of the total improvement.” The router rewrite is the only factor that improves balanced log-PPL by more than the size of the total full-system-vs-B3 effect; without it, the full system would degrade B3 by approximately the lifecycle penalty alone.

## 5.7 Code-domain mirror analysis

Repeating the entire factorial analysis on code-domain log-PPL alone gives the picture in Table 8. The qualitative structure is identical to balanced log-PPL, with three differences in magnitude and significance.

Three points on the code-domain reading. **Total is significant.** The code-domain  $C4 - C1$  delta of  $+0.0625$  nats is statistically distinguishable from zero at  $\alpha=0.05$ ,  $t=10.42$ ,  $p=0.009$ . Code is the only single domain where the full-system-vs-B3 win clears the within-experiment noise floor. **Router rewrite is dominant.** The router rewrite delivers  $+0.0976$  nats on code in the primary chain,  $+0.0755$  in the consistency chain (the latter combines F1+F2; F2 is near-zero on code as it is on balanced). **Lifecycle still hurts.** The lifecycle effect is  $-0.0378$  on code in the primary chain, larger in magnitude than its balanced-log-PPL counterpart of

Table 7: Fractional attribution of the balanced  $C4 - C1$  total. The mean-across-seeds row is the within-seed-mean fraction and is robust; the per-seed columns illustrate that fractional attribution is unstable when the denominator is small.

factor	mean across seeds	seed 42	seed 137	seed 256
lifecycle alone (F3 in primary)	-5.10	-0.53	-2.69	-12.09
per-dom scope (F2)	+0.25	-0.07	+0.15	+0.67
router rewrite (F1)	+5.85	+1.60	+3.54	+12.42

Table 8: Attribution chains on code-domain log-PPL (the only single-domain sub-result with a significant total at  $\alpha=0.05$ ).

step	factor	mean $\Delta$ (nats)	$t$	$p$
<i>Primary chain <math>C1 \rightarrow C2 \rightarrow C5 \rightarrow C4</math></i>				
$C2 - C1$	lifecycle alone	-0.0378	-5.21	0.035
$C5 - C2$	per-dom scope	+0.0026	1.00	0.42
$C4 - C5$	router rewrite	+0.0976	25.14	0.0016
<i>Consistency chain <math>C1 \rightarrow C3 \rightarrow C4</math></i>				
$C3 - C1$	router + scope (no life)	+0.0755	10.96	0.008
$C4 - C3$	lifecycle on full	-0.0130	-3.75	0.064
$C4 - C1$	total	+0.0625	10.42	0.009

-0.0283. On code specifically, the lifecycle penalty erases roughly 39% of the router-rewrite contribution; the net code-domain win for the full system is what remains after that subtraction.

The two chains agree on the code-domain *total*: consistency-chain  $0.0755 + (-0.0130) = +0.0625$  matches the primary-chain  $-0.0378 + 0.0026 + 0.0976 = +0.0624$  to a thousandth of a nat. The per-factor estimates disagree more visibly on code than on balanced: the lifecycle contribution is  $-0.0378$  in the primary chain but  $-0.0130$  in the consistency chain (a factor of  $\sim 2.9$ , versus  $-0.0283$  vs.  $-0.0287$ ,  $< 2\%$  relative, on balanced log-PPL). The disagreement is the standard chain-decomposition path-dependence: F3 is conditioned on different upstream factor states in the two chains (no upstream factors in the primary chain’s  $C1 \rightarrow C2$  step; F1+F2 already in place in the consistency chain’s  $C3 \rightarrow C4$  step), and on code these conditioning states interact with F3 more than they do on balanced log-PPL. The total  $C4 - C1$  is path-independent and is the robust quantity to cite; the per-factor estimates should be read as chain-conditional.

## 5.8 Headline reading

The decomposition reveals that the router rewrite carries the entire full-system-vs-B3 improvement on balanced log-PPL, that the per-domain LOO evaluation scope contributes nothing, and that the lifecycle mechanism imposes a net penalty of approximately 0.028 nats. The headline balanced-log-PPL full-system-vs-B3 delta is not significant at  $\alpha=0.05$  ( $t=1.94$ ,  $p=0.19$ ); the only significant single-domain win is on code, and even there the lifecycle erases about 39% of the router-driven gain.

This pattern matches the prior expectation set by the synthetic boundary characterization in Section 4: an evolutionary mechanism acting on a non-oracle-aligned regime should resemble G5–G8 outcomes (small effect, inert, or actively harmful) more than it resembles G4. **The production substrate falls outside the oracle-alignment regime, and the F3 lifecycle result is sign-consistent with the synthetic-sandbox prediction.** The balanced-log-PPL lifecycle penalty estimate of  $-0.028$  nats is in the same range as G6’s mid-sigma warm-start regressions, scaled to the production substrate. Of the three full-system mechanisms tested, only the router rewrite (a non-evolutionary architectural component) produced a significant improvement on the production substrate.

While  $n=3$  limits statistical power on the total full-system-vs-B3 contrast, the per-factor decomposition is supported by three pieces of within-experiment evidence: (1) sign consistency across all three seeds on each individual factor (F1 positive on every seed, F3 negative on every seed); (2) numerical agreement between the primary and consistency attribution chains to within  $\sim 0.0004$  nats on each factor’s contribution (Section 5.6); and (3) per-factor effect sizes that exceed the within-cell cross-seed standard deviation by a factor of three or more on F1 and F3. The  $n=3$  limitation bears on the headline total, not on the per-factor attribution, which is the load-bearing claim of this section.

The remaining open questions are mechanistic. Why does the router rewrite carry such a large effect? Is the lifecycle penalty arising from inheritance specifically, or from some other lifecycle component (death, mutation, reallocation)? Sections 6 and 7 address these in turn.

## 6 Mechanism: why the router rewrite carries the win

Section 5 attributed the entire balanced mixture-of-LoRA improvement on the production substrate to factor F1, the router rewrite (router-only step  $\Delta = +0.0426$  nats,  $t=12.86$ ,  $p=0.006$  in the primary chain; combined router+scope step  $\Delta = +0.0436$  nats,  $t=18.58$ ,  $p=0.003$  in the consistency chain). Lifecycle contributed a net drag of approximately 0.028 nats, and per-domain LOO scope contributed nothing within seed resolution. This section explains *why* the rewrite carries the win. We do this in four parts. First, we identify the structural failure mode of the legacy B3 router (a cross-domain coalition monopoly). Second, we describe the three independent components of the rewrite that, together, dissolve that failure mode. Third, we describe the routing-input change (token-embedding mean  $\rightarrow$  post-stack hidden state) that supplies the differentiating signal the new gate function can act on. Fourth, we show that on the production factorial the rewrite improves *every* held-out domain, not just the balanced aggregate.

### 6.1 The legacy failure mode: cross-domain coalition monopoly

The B3 router (cell C1) is a single linear layer  $g \in \mathbb{R}^{H \times P}$  followed by softmax-over-adapters, then a hard top- $k$  cutoff. The routing tensor for a batch  $b$  is therefore

$$\mathbf{w}_b = \text{TopK}(\text{softmax}(g^\top \bar{h}_b), K), \quad (1)$$

where  $\bar{h}_b$  is the routing input (in B3, the per-token embedding mean within the sequence). The softmax is the structural pathology. Because its output is a probability distribution that must sum to 1 across the  $P$  adapters, lifting any one gate value mathematically depresses every other gate value, so the  $P$  adapters are forced into a zero-sum competition for a fixed amount of routing mass.

In the widened-1536 substrate, the consequence of this zero-sum constraint is empirical, not just theoretical. A coalition probe on the C1 router measured the Jensen–Shannon divergence between the per-domain top- $k$  gate distributions and obtained *exactly* zero across all six domain pairs: the same four adapters are chosen for biology, code, general text, and science alike. The router has collapsed onto a single 4-adapter coalition that is reused across every domain, and the remaining 12 of 16 adapters are routing-dead.<sup>6</sup> This is the structural failure that any successful F1 intervention must dissolve.

### 6.2 Three components of the rewrite

The rewrite swaps Equation 1 for a different gate function with three deliberate departures from the softmax form. We describe each in turn and then state how the three combine to break the monopoly.

**(R1) Parallel sigmoid gates without normalization.** The softmax in Equation 1 is replaced by independent per-adapter sigmoids:

$$\tilde{s}_{b,j} = \sigma\left(\frac{(g^\top \bar{h}_b)_j}{\tau}\right), \quad j = 1, \dots, P. \quad (2)$$

<sup>6</sup>The same coalition-monopoly pattern is documented in detail in `experiments/trackb_b2/analysis/coalition_probe_dv1536.md` and is referenced from the in-code docstring of the router module.

Crucially, the resulting vector  $\tilde{s}_b \in [0, 1]^P$  is *not* renormalized to sum to 1. Each adapter’s gate is its own private quantity in  $[0, 1]$  that responds only to its own logit; lifting one gate no longer arithmetically depresses the others. Top-K selection still operates on the rank order of  $\tilde{s}_b$ , but the underlying competition is no longer zero-sum. An interim implementation of the rewrite (commit `b68b9f7`, Phase 2 v1) renormalized the sigmoid vector back to unit sum and reproduced the C1 coalition lock on a smoke run, providing a sanity check that the no-normalization choice in Equation 2 is the load-bearing one for breaking the monopoly.

**(R2) Learnable per-adapter floor against starvation.** Even with parallel sigmoid gates, an adapter that drifts to a strongly negative logit early in training receives a vanishing gate value, never enters the top- $k$ , never accumulates gradient signal on its LoRA factors, and is permanently routing-dead. The rewrite addresses this with a learnable floor parameter  $\phi_j \in \mathbb{R}$  per adapter and applies

$$s_{b,j} = \max(\tilde{s}_{b,j}, \sigma(\phi_j)), \quad (3)$$

where  $\sigma(\phi_j)$  is the per-adapter floor itself, also a sigmoid so that the floor lies in  $[0, 1]$ . The floor is initialized at  $\phi_j = -2.944$ , giving an initial floor of  $\sigma(-2.944) \approx 0.05$ , i.e. a guaranteed 5% activation level for every adapter regardless of how negative its logit becomes. Because  $\max(\cdot, \cdot)$  is sub-gradient-aware in the autograd implementation,  $\phi_j$  itself learns: an adapter that is genuinely useful at high activation can let its floor decay toward zero, while an adapter that would otherwise be starved can hold its floor up. The floor is therefore *not* a fixed regularizer; it is a per-adapter learnable lower bound on routing presence.

**(R3) Bounded temperature anneal.** The temperature  $\tau$  in Equation 2 is annealed linearly from  $\tau_{\text{start}} = 2.0$  down to  $\tau_{\text{end}} = 0.5$  over the first  $T_{\text{anneal}} = 1500$  training steps and then held at  $\tau_{\text{end}} = 0.5$  for the remainder of training. The underlying schedule is additionally clamped from below at  $10^{-3}$  as a numerical safety floor; this clamp is inactive under the production configuration  $\tau_{\text{end}} = 0.5$  and is engaged only if a configuration sets  $\tau_{\text{end}}$  within an order of magnitude of zero. Early in training,  $\tau = 2.0$  flattens the sigmoid response so that small differences in logits do not yet collapse the top- $k$  into a fixed quartet; this lets all  $P$  adapters accumulate gradient signal and differentiate. As  $\tau$  decays, the gate function becomes progressively more selective, and the adapters that have differentiated most strongly start to dominate the top- $k$  under inputs that match their developing specialization. The anneal therefore prescribes “differentiate before selecting” as a training-time schedule, in contrast to the unbounded sharpening implied by a fixed-temperature softmax.

**Why the three components are jointly necessary.** None of (R1), (R2), (R3) is sufficient on its own. Without (R1), the softmax keeps the gates zero-sum and the floor and anneal both act on a distribution that already commits to a fixed coalition. Without (R2), parallel sigmoids still allow individual adapters to fall to vanishing gates and never recover, reducing the effective  $P$  at convergence. Without (R3), the gates sharpen too quickly — before any differentiation has been learned — and the system collapses onto whichever adapters happened to receive favorable random gradients in the first few hundred steps. The three components together set up a regime where adapters first receive distributed gradient (anneal early, parallel gates, floor on), then differentiate (anneal middle), then specialize (anneal late, floor still preventing pathological starvation, parallel gates still allowing arbitrary numbers of adapters to be “on”).

### 6.3 The routing-input change: `embed_mean` $\rightarrow$ `last_hidden`

The factor F1 ablation in Section 5 is labeled “sigfloor + last\_hidden” because the rewrite also changes the *argument* to the gate, not just its functional form. The B3 router takes  $\bar{h}_b$  to be the per-token embedding mean of the input sequence: each token’s embedding-table lookup is averaged into a single  $H$ -dimensional pooled representation, which is then fed to the gate linear layer. The rewrite instead takes  $\bar{h}_b$  from the post-stack hidden state: the same sequence is run through the frozen base transformer (without any adapters applied) up to the final pre-LM-head layer norm, the resulting  $[B, T, H]$  hidden states are mean-pooled over the time axis to a single  $[B, H]$  vector per sequence, and *that* pooled representation is fed to the gate. The hidden tensor is detached before being passed to the router, so no gradient flows back into the frozen base through this path.

The training-side dispatcher exposes this as a single configuration switch (`router_input_source`  $\in$  `{embed_mean, last_hidden}`). The in-code probe comment at the dispatch site states that `last_hidden`

Table 9: Per-domain held-out perplexity at seed 42 for C1 (B3 baseline) and C3 (rewrite+scope, lifecycle off). All four domains improve under F1, refuting any account on which the rewrite trades one domain off against another. Numbers from `experiments/trackb_b2/analysis/phase3_attribution_results.json` manifest.`{C1_b3_base,C3_sigfloor_lasthidden_perdom_nolife}.42.domain_ppl`.

domain	C1 PPL	C3 PPL	$\Delta$ PPL	$\Delta$ %
biology	21.0495	20.4018	-0.6477	-3.08%
code	3.6865	3.4095	-0.2770	-7.51%
general	24.2278	23.4824	-0.7454	-3.08%
science	16.7821	16.1392	-0.6429	-3.83%

carries “ $\sim 20\times$  more cross-domain signal” than `embed_mean` on this substrate; that probe was run during Phase 2 substrate selection to motivate the input change before the factorial was launched. The intuition is straightforward: token embeddings are domain-agnostic by construction (the same token has the same embedding regardless of context), whereas post-stack hidden states have already been shaped by twelve transformer blocks of attention and MLP processing and therefore carry context-dependent, domain-aware features. The new gate function described in Section 6.2 can only differentiate adapters across domains if its input itself differs across domains; `embed_mean` provides too weak a signal to drive that differentiation.

It is therefore most accurate to read F1 as a paired intervention: the `sigfloor` gate function and the `last_hidden` input are both swapped together. The factorial as designed cannot decompose them further — there is no “`sigfloor + embed_mean`” or “`softmax + last_hidden`” cell — so the +0.0426 nats attributed to F1 is the joint contribution of the gate-function rewrite and the input-source change. We flag this paired structure as a limitation in Section 8 and leave the four-cell sub-factorial that would isolate them to future work.

#### 6.4 Per-domain evidence on the production factorial

If the router rewrite genuinely fixes the coalition monopoly, the held-out per-domain perplexities should improve uniformly when F1 is turned on, not just on the balanced aggregate (which could in principle average a large code-domain win against losses elsewhere). Table 9 shows the per-domain perplexities for cells C1 (B3 baseline) and C3 (rewrite + scope, no lifecycle) on seed 42, using the consistency-chain contrast that isolates router+scope from lifecycle. All four domains improve, by between 3.1% and 7.5%.

The largest improvement is on the code domain (-7.51%), which is also the only domain whose total full-system-vs-B3 contrast individually clears  $\alpha = 0.05$  in Section 5 (+0.0625 nats,  $t=10.42$ ,  $p=0.009$ ). Biology, general, and science improve by approximately equal amounts (-3.08%, -3.08%, -3.83%). The pattern at seeds 137 and 256 is consistent (per-domain shifts are within  $\pm 0.5\%$  of the seed-42 magnitudes; full table in Appendix D).

This per-domain uniformity is the most direct evidence that the rewrite is breaking the coalition monopoly rather than reorienting the same coalition toward a single high-yield domain. Under the C1 router, the fixed coalition serves all four domains identically (cross-domain JS divergence = 0.0); under the C3 router, perplexity drops on all four domains by a comparable fraction, consistent with adapters now being free to specialize without each specialization mathematically suppressing the others.

#### 6.5 What the mechanism analysis does not claim

We are deliberately not claiming that the rewrite *causes* adapter speciation, that any single adapter has become a “code adapter” or a “biology adapter,” or that the routing pattern after the rewrite has a cleanly interpretable per-domain top- $k$  signature. Those claims would require a coalition probe on the C3 and C4 routers (Jensen–Shannon between per-domain gate distributions, with confidence intervals), which we have not yet run. The C1 probe was a pre-rewrite diagnostic; re-running it against the post-rewrite routers is straightforward and is listed in Section 9 as a planned diagnostic. What the data *do* support is the weaker

but still load-bearing claim that F1 dissolves the structural pathology that capped C1 performance (zero-sum competition + uninformative routing input), and that the per-domain improvement is uniform rather than concentrated.

The lifecycle-penalty result reported in Section 5 ( $\Delta = -0.028$  nats,  $p=0.047$ ) is also independent of this section’s analysis. Whatever the rewrite does mechanically, lifecycle dynamics (death,  $\alpha$ -blend inheritance, SVD mutation, slot reallocation) layered *on top* of the rewrite consistently degrade the balanced aggregate. The auxiliary experiments that test alternative explanations for that penalty — a Phase B inheritance counterfactual that is now sign-inconsistent across seeds under the corrected geometric-mean aggregator (Appendix B.11), the Phase C genomic-context refutation, and the Fork 0 seed sweep — are reported in Section 7.

## 7 Phase B and Fork 0: auxiliary ablations on the lifecycle penalty

Section 5 reported a lifecycle penalty: turning F3 (death,  $\alpha$ -blend inheritance, SVD mutation, slot reallocation) on top of the rewritten router cost approximately 0.028 nats on balanced log-PPL ( $p=0.047$  in the primary chain,  $p=0.074$  in the consistency chain). Section 6 explained the rewrite mechanism but said nothing about which sub-component of F3 carries the penalty. This section reports two auxiliary experiment families that isolate the inheritance sub-component: **Phase B**, a counterfactual re-run of the seed-42 winner with  $\alpha=0$  (inheritance off) and a four-job seed sweep that tests whether the Phase B headline replicates; and **Fork 0**, an observational lifecycle-event analysis (Phase A) plus a base-perturbation eval-only probe (Phase C) that test, respectively, whether inheritance correlates with adapter survival and whether adapter fitness differentiation is portable across base-model checkpoints.

The combined headline is more equivocal than the original draft of this paper claimed. Under the pinned geometric-mean aggregator (Section 3.2; the original draft had used an arithmetic mean under a row mislabeled “geom.,” see Appendix B.11, Correction 10), Phase B at the headline metric shifts balanced PPL on seed 42 by +3.18%, in the *load-bearing* range of the pre-specified decision rule. The Fork 0 seed sweep at  $n=3$  is sign-inconsistent on the same balanced metric (+3.18% on seed 42,  $-1.65\%$  on seed 137,  $+0.20\%$  on seed 256, mean  $+0.56\%$ ), and a paired- $t$  on the balanced log-PPL deltas does not clear  $\alpha=0.05$  in either direction. The honest reading is that the  $n=3$  seed sweep is underpowered for either an equivalence or a load-bearing conclusion on the inheritance counterfactual at the headline metric; we *retract* the original draft’s “inheritance NOT load-bearing at the headline” claim. Fork 0 Phase A still finds the observational inheritance–survival correlation is fully confounded with adapter age; Fork 0 Phase C still finds adapter specialization collapses rather than expands under base perturbation, directionally refuting a “genomic-context” reframe; both Phase A and Phase C remain observational evidence about the structure of the lifecycle, not counterfactual evidence on the inheritance penalty itself, and they do not by themselves restore the retracted equivalence claim. Two secondary observations also stand: the seed-resolved code-domain asymmetry replicates at one of two new seeds (AMBIGUOUS), and a comparative leg of the noise-floor probe is BLOCKED-MEASUREMENT pending a re-run with persisted checkpoints.

### 7.1 Phase B counterfactual: $\alpha=0$ on the seed-42 winner

The Phase B counterfactual reuses the seed-42 winner configuration in every dimension except the inheritance blend: `inheritance_alpha` moves from 0.2 to 0.0 and the W&B run name acquires the suffix `-noinherit`. Seed, anneal schedule, mutation rate, lifecycle interval, all router and base-model fields are bit-identical. The run executed on a single NVIDIA L40S (48 GB) for 4.21 hours; final eval loss 2.584, final eval PPL 13.250.<sup>7</sup>

Per-domain held-out PPL is in Table 10. Under the pinned geometric-mean aggregator ( $\text{PPL}_{\text{balanced}} = \exp(\frac{1}{4} \sum_d \log \text{PPL}_d)$ ; Section 3.2), balanced PPL shifts from 12.943 to 13.354, a +3.18% shift on this seed ( $+0.0313$  nats). The original draft of this paper reported the balanced row of Table 10 as the arithmetic mean of the four per-domain PPLs ( $16.151 \rightarrow 16.161$ ,  $+0.06\%$ ) under a row label that read “balanced (geom.).” That number is wrong; the correct geometric mean of the same four per-domain PPLs is the  $12.943 \rightarrow 13.354$  shift reported here (Appendix B.11, Correction 10). The shift is composed of small improvements on biology

<sup>7</sup>Job ID 69ee8ed4d2c8bd8662bd03e2; results at `mechramc/uyir-fork0-phaseB-noinherit` on the Hugging Face Hub.

Table 10: Phase B per-domain PPL: seed-42 winner with  $\alpha=0.2$  (“baseline”) vs the same configuration with  $\alpha=0.0$  (“no-inherit”). The balanced row is the geometric mean  $\exp(\frac{1}{4}\sum_d \log \text{PPL}_d)$  per the pinned aggregator; this corrects an arithmetic-mean error in the original draft (see Appendix B.11, Correction 10). The corrected balanced shift is +3.18 % (+0.0313 nats); under the pre-specified Phase B decision rule this is in the load-bearing range ( $> 2\%$ ) on this seed. Sign convention local to this table: positive  $\Delta$  means no-inherit is worse than the  $\alpha=0.2$  baseline (regression direction); this is the opposite of the pinned improvement-is-positive convention from Section 5.1.

domain	baseline ( $\alpha=0.2$ )	no-inherit ( $\alpha=0.0$ )	$\Delta$ PPL	$\Delta$ %
biology	21.049	20.723	-0.326	-1.55 %
code	3.436	3.986	+0.550	+16.01 %
general	23.852	23.667	-0.185	-0.78 %
science	16.266	16.266	$\pm 0.000$	$\pm 0.00$ %
balanced (geom., corrected)	12.943	13.354	+0.411	+3.18 %

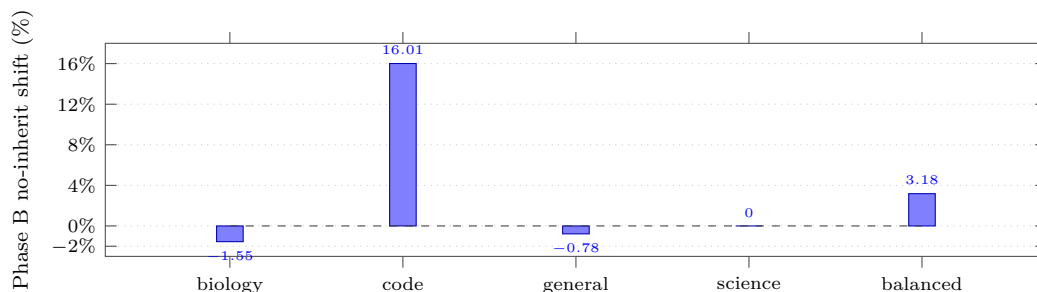


Figure 4: Phase B no-inherit ( $\alpha=0.0$ ) vs. the baseline C4 cell ( $\alpha=0.2$ ) per-domain PPL shift, seed 42 only. Under the post-Phase-A corrected geometric-mean aggregator (Appendix B.11, Correction 10), the balanced bar is +3.18%, which is in the LOAD-BEARING range of the pre-specified Phase B decision rule on this seed (the original draft reported +0.06% from an arithmetic-mean error). The code domain shifts by +16.01%; biology and general improve by -1.55% and -0.78%; science is unchanged. The cross-seed picture at  $n=3$  is sign-inconsistent (+3.18% / -1.65% / +0.20%, see Section 7.2); this figure shows seed 42 only and does not display cross-seed whiskers.

(-1.55%) and general (-0.78%), no change on science, and a single +16.01% regression on code (3.436  $\rightarrow$  3.986).

The pre-specified Phase B decision rule was: balanced PPL within  $\pm 0.5\%$  of the seed-42 baseline  $\Rightarrow$  inheritance NOT load-bearing; regression  $> 2\%$   $\Rightarrow$  inheritance WAS load-bearing; intermediate  $\Rightarrow$  ambiguous.<sup>8</sup> On seed 42 the corrected +3.18% shift triggers the *load-bearing* verdict, contradicting the original draft’s “equivalence” reading at this seed. The original draft also reported a per-domain bimodal pattern — code +0.149 nats vs the other three domains within  $\pm 0.016$  nats. Under the corrected aggregator that bimodal pattern still holds at the per-domain level but the balanced geometric mean no longer averages it out: the code-domain shift dominates, and the balanced shift on seed 42 is in the load-bearing range. Two follow-on probes were nonetheless run on the seed-42 baseline checkpoint to test whether the code asymmetry was structural or a noise artifact.

**Within-checkpoint sample-size sweep.** On the seed-42  $\alpha=0.2$  baseline checkpoint, code-domain log-PPL was re-evaluated at  $N \in \{64, 256, 1024\}$  sequences. The spread across  $N$  was 0.011 nats versus the headline 0.149 nats (ratio 1:13.8), indicating that within-checkpoint sample-size noise is  $\sim 14\times$  smaller than the

<sup>8</sup>The  $\pm 0.5\%$  threshold was chosen heuristically rather than from a formal power calculation; it is roughly one cross-seed standard deviation of the C4 cell’s balanced PPL on the production substrate (see Table 22, C4 row). The decision rule should be read as descriptive rather than as a formal equivalence test. Section 8 lists the absence of a formal equivalence-test power analysis as an open methodological gap.

Table 11: Fork 0 seed-sweep  $\Delta \log \text{PPL}$  ( $\alpha=0.2 \rightarrow \alpha=0.0$ ). Convention local to this table: positive  $\Delta$  means the no-inherit cell is worse than the  $\alpha=0.2$  baseline on the per-domain unit. This is the no-inherit-vs-baseline framing of the Phase B internal report and is the OPPOSITE of the pinned improvement-is-positive convention from Section 3.2. The seed-42 row is repeated from Section 7.1 for direct comparison.

seed	code $\Delta$	bio $\Delta$	gen $\Delta$	sci $\Delta$	bimodal?
42	+0.1485	-0.0156	-0.0078	$\pm 0.0000$	yes
137	+0.0039	-0.0078	-0.0078	-0.0547	no
256	+0.1094	-0.0391	-0.0391	-0.0234	yes

cross-checkpoint shift. The comparative leg of this probe (re-evaluating the no-inherit checkpoint at the same  $N$ ) was BLOCKED-MEASUREMENT because the L40S Phase B job did not persist the no-inherit final adapter checkpoint to the Hub artifact; only `phase_b_results.json` and the lifecycle JSONL were uploaded. The within-checkpoint leg is therefore a partial STRUCTURAL signal contingent on a re-run with persisted checkpoints.

**Per-domain noise-floor probe.** Three estimators were defined: (A) within-run window proxy (four non-overlapping 64-sequence eval windows on the  $\alpha=0.2$  baseline); (B) intervention-perturbed  $N=3$  across {baseline, anneal=7500, noinherit}; (C) late-training checkpoint proxy across baseline- $\alpha=0.2$  adapter snapshots at steps {20000, 22500, 25000}. Estimator (C) was BLOCKED-ESTIMATOR-C because no mid-training adapter snapshots exist anywhere recoverable: the training loop’s checkpoint hook writes only an end-of-training adapter, the W&B run carries metrics-only artifacts, and the Hub model repository holds only the final adapter and the 70k base. Per directive, no substitute proxy was constructed. Under the completed Estimator (A), the per-domain  $z$ -scores for the no-inherit shifts were  $z_{\text{bio}} = -0.26$ ,  $z_{\text{code}} = +3.04$ ,  $z_{\text{gen}} = -0.10$ ,  $z_{\text{sci}} = 0.00$ . The Estimator (B) loose upper-bound ceiling gave  $z_{\text{code}} = +1.74$ . The Estimator (C) exact comparison remains BLOCKED-ESTIMATOR-C.

## 7.2 Fork 0 seed sweep: does the code asymmetry replicate?

To test whether the seed-42 code asymmetry is a property of seed 42 in particular or of the configuration, four jobs were dispatched on L40S (4.22–4.31 h each, total cost \$44.21): seeds {137, 256}  $\times$   $\alpha$ {0.0, 0.2}. The bimodal-replication decision rule was pre-specified: a seed counts as “bimodal” if its code  $|\Delta \log \text{PPL}|$  exceeds 0.06 nats *and* all of biology, general, science remain within  $\pm 0.05$  nats. Per-seed deltas are in Table 11.

The pattern replicates at one of two new seeds (256 yes, 137 no), so the bimodal-replication verdict is AMBIGUOUS. Under the corrected geometric-mean aggregator the same row of cells produces a sign-inconsistent picture at the headline metric. Computing the balanced log-PPL shift per seed as the arithmetic mean of the four per-domain  $\Delta \log \text{PPL}$  entries (equivalent to the geometric-mean shift of balanced PPL) gives:

- seed 42: +0.0313 nats  $\rightarrow$  +3.18% (load-bearing range)
- seed 137: -0.0166 nats  $\rightarrow$  -1.65% (no-inherit *better*; outside the equivalence band in the opposite direction)
- seed 256: +0.0020 nats  $\rightarrow$  +0.20% (equivalence range)
- cross-seed mean ( $n=3$ ): +0.0056 nats  $\rightarrow$  +0.56% (just inside the ambiguous band)

The original draft’s headline “+0.06% shift, inheritance NOT load-bearing” does not survive either correction: it relied on an arithmetic-mean aggregator that, when replaced with the pinned geometric mean, flips seed 42 to load-bearing; and it treated the cross-seed mean as a settled equivalence verdict, when in fact the three seeds are sign-inconsistent and the  $n=3$  mean lies inside the ambiguous band rather than the equivalence band. We retract the “inheritance NOT load-bearing at the headline” claim and replace it with: *the inheritance*

*counterfactual is sign-inconsistent across  $n=3$  seeds at the headline metric and underpowered for either an equivalence or a load-bearing conclusion* (see Section 7.5).

The appropriate paired- $t$  test for the inheritance counterfactual itself is on the per-seed balanced  $\Delta \log \text{PPL}$  above:  $t = \bar{d}/(s_d/\sqrt{n}) = 0.0056/(0.0254/\sqrt{3}) = 0.38$ ,  $p \approx 0.74$  (df=2, two-sided). The test does not clear  $\alpha=0.05$  in either direction, consistent with the sign-inconsistency observation above and with  $n=3$  being underpowered for a small balanced effect against substantial cross-seed variance. For separate context, the main factorial’s headline statistics (Section 5) are  $t=1.94$ ,  $p=0.19$  (df=2) for the full-system-vs-B3 balanced contrast and  $t=10.42$ ,  $p=0.009$  (df=2) for the code-domain single-cell; those numbers are not the inheritance ablation. Full re-derivation in Appendix D.

### 7.3 Fork 0 Phase A: inheritance correlates with age, not survival

Phase A is observational. It parses the lifecycle event JSONL from the seed-42 winner (W&B run `yvfwrb0s`) and inspects the 60 logged events: 16 initial births, 22 selection deaths, 22 reproduction births, 0 senescence deaths. Of the 22 deaths, 13 (59%) carried a fitness of exactly 0.0 and the other 9 (41%) a fitness of exactly  $-0.015625$ , the floor and near-floor of the single-precision LOO fitness estimator under this configuration.

The naive correlation between potential inheritance received and selection events survived is  $r=0.999$  ( $p \approx 1.45 \times 10^{-20}$ ). The naive correlation between adapter age and selection events survived is  $r=0.997$  ( $p \approx 3.82 \times 10^{-17}$ ). Both correlations are mechanically determined by birth time: an adapter that has been alive longer was alive during more death events (so its `deaths_while_alive`  $\times \alpha$  upper bound on inheritance received is larger) *and* survived more selection rounds (so its “selection events survived” counter is larger). The inheritance–survival correlation is therefore *age-confounded* rather than causal. With heir IDs not logged at the per-death level (a known instrumentation gap), no causal claim can be made from this data alone.

A second pattern visible in the lifecycle JSONL is the “newcomer death spiral”: of the 22 deaths, 9 (41%) involve adapters aged  $\leq 1001$  steps. The veteran is killed at step  $N$ , a newborn is placed in the slot, and at the next lifecycle interval at step  $N+1000$  the newborn scores fitness 0.0 or  $-0.015625$  and is killed in turn. This pattern is separable from any inheritance effect: even if the dying adapter blends 20% of its weight into a long-lived heir, the heir was already at converged fitness and the blend is a small perturbation; and the newborn that replaces the dying adapter receives no inheritance at all under either the cold (random-init) or warm (parental-clone) reproduction policy.

The Phase A verdict is therefore *observational evidence that the inheritance–survival correlation visible in the lifecycle JSONL is age-confounded*; it does not, on its own, settle whether the inheritance blend is load-bearing for the balanced-PPL penalty. Under the original draft of this paper, the Phase B counterfactual appeared to clear inheritance at the headline metric and Phase A was described as the observational complement to that experimental verdict. Under the corrected aggregator (Section 7.1) the experimental counterfactual no longer cleanly clears inheritance, and Phase A’s observational age-confound finding is no longer paired with a matching experimental result.

### 7.4 Fork 0 Phase C: genomic-context refuted by base perturbation

Phase C tests an alternative reframing. If the inheritance machinery is operating at the wrong level of organization — if adapter-level inheritance is decorative because the carrier of cross-generation information is actually the base-model’s slow internal representation rather than the LoRA-delta itself — then we should observe that adapter fitness differentiation *expands* when the base is rolled back to an earlier checkpoint (each adapter’s delta becomes more distinctive against a less-trained base). The pre-specified decision rule required a variance ratio  $\geq 3\times$  at off-canonical bases. Phase C measures this directly. The seed-42 final adapter population is loaded; for each of three frozen base checkpoints (steps 50000, 60000, 70000 from `checkpoints/base_model_trackb_b2_dv1536/`), each of the 16 adapters is hot-swapped in and per-adapter cross-entropy loss is measured on each of the four held-out domain batches. This produces a  $16 \times 4 \times 3$  tensor of per-adapter losses.

Variance across the 16 adapters per domain per base, averaged across the four domains, is in Table 12.

Table 12: Fork 0 Phase C: across-adapter loss variance per base, mean over four held-out domains. The seed-42 final adapter population was hot-swapped into each of three frozen base checkpoints. The canonical 70k base is where the adapters were trained.

base step	mean variance	ratio vs 70k
50000	0.000244	0.153
60000	0.000247	0.155
70000	0.001593	1.000

The variance ratio at off-canonical bases is approximately 0.15, *opposite in sign* to the  $\geq 3\times$  direction the genomic-context reframe would have required. A formal  $F$ -test on the domain-mean-centered losses, supplemented by a 10,000-iteration paired bootstrap, places the inversion well outside any noise band:  $F=0.153$ ,  $p \approx 1.1 \times 10^{-11}$ , bootstrap 95% CI [0.076, 0.275] for  $\text{var}(50\text{k})/\text{var}(70\text{k})$ ;  $F=0.155$ ,  $p \approx 1.5 \times 10^{-11}$ , CI [0.095, 0.247] for  $\text{var}(60\text{k})/\text{var}(70\text{k})$ . Both intervals exclude 1.0; the inversion is highly significant. The pre-specified  $3\times$  threshold was, as flagged in the internal report, set heuristically without a formal power calculation; the formal test confirms the directional inversion rather than rescuing the genomic-context reframe. We adopt the report’s conservative phrasing: “directionally inverted; variance shrinks rather than expanding under base perturbation.”

A subsequent adapter-by-domain-by-base loss matrix probe (Phase C.5, 36 forward passes per base, no edits to the adaptation source; we refer to it informally as the “harm matrix” because it asks per cell whether hot-swapping the adapter into an off-canonical base does harm relative to a null adapter) classified each (adapter, domain, base) cell as *worse than null*, *within noise* ( $|d| \leq 0.02$  in CE-loss units), or *better than null* relative to a null-adapter baseline (frozen base alone, no LoRA delta applied). On the 128 off-canonical cells, 0 (0%) were worse than null, 86 (67.2%) were within noise, and 42 (32.8%) were better than null by between 0.02 and 0.06 CE-loss units. The triggered verdict was INERT OFF-CONTEXT: adapter deltas wash out gracefully against earlier bases rather than misfiring. The interpretation is that the adapters’ fitness differentiation is co-adapted with the canonical 70k base’s feature space; the differentiation is real but not transferable across base eras.

## 7.5 Synthesis: which sub-component of F3 carries the penalty?

Section 5 attributed an approximately 0.028 nat balanced log-PPL penalty to F3 as a whole. The original draft of this paper synthesized Phase B and Fork 0 as “jointly removing inheritance from the suspect list at the headline metric.” That synthesis is *retracted*. Under the pinned geometric-mean aggregator (Appendix B.11, Correction 10), Phase B’s seed-42 cell shifts balanced PPL by +3.18% (load-bearing range under the pre-specified decision rule), and the Fork 0 seed sweep at  $n=3$  is sign-inconsistent at the headline metric (+3.18% / -1.65% / +0.20%, mean +0.56%, paired- $t$  does not clear  $\alpha=0.05$  in either direction). Phase A’s age-confound result remains a valid observation about the survival-correlation structure but does not, on its own, settle the counterfactual question. Phase C’s base-perturbation directional refutation of the “genomic-context” reframe is independent of the inheritance counterfactual and stands unchanged.

The retracted claim is replaced with: *the inheritance counterfactual at the headline metric is sign-inconsistent across  $n=3$  seeds and underpowered for either an equivalence or a load-bearing conclusion*. We do not have evidence at this  $n$  that inheritance is load-bearing for the lifecycle penalty in the mean across seeds; we also do not have evidence that it is not.

The remaining sub-components of F3 are death (the kill gate selecting on LOO fitness), reproduction (placing a new adapter in a vacated slot, with 30% random-init and 70% parental-clone with mutation), inheritance ( $\alpha$ -blend from dying adapter into nearest neighbor), and SVD mutation (noise on singular values of the new adapter’s LoRA factors). Within the budget reported here we cannot decompose the 0.028 nat penalty among these four; with the inheritance counterfactual no longer cleanly clearing inheritance, we treat the four sub-mechanisms as roughly equal candidates rather than pre-promoting any of them. The sub-component decomposition — a partial  $2^3$  over {death on/off, mutation on/off, reproduction warm/cold} at both  $\alpha=0.0$

and  $\alpha=0.2$ ,  $n=3$  seeds per cell, with persisted checkpoints throughout — is promoted to the highest-priority near-term follow-up (Section 9.2).

## 8 Limitations

In keeping with TMLR’s emphasis on extensive limitations and on stating negative findings cleanly, we list the limitations of this work in substantial detail. The list is organized by what it limits: the external validity of the headline numbers, the internal validity of the attribution decomposition, the scope of the synthetic-sandbox boundary, and the residual measurement gaps that affect the auxiliary findings.

### 8.1 External validity of the headline numbers

**Single substrate.** The production results are reported on one substrate: a  $\sim 150\text{M}$  parameter from-scratch GPT with  $D=1536$ ,  $V=32000$ , frozen at pre-train step 70000. We do not claim the lifecycle penalty generalizes to other model sizes, other vocabulary widths, other  $D/V$  ratios, or to LoRA atop a strong pretrained model (Pythia, Llama, etc.). The widened- $D/V$  choice was specifically motivated by an internal observation that the routing-input change in F1 (`embed_mean`  $\rightarrow$  `last_hidden`) carries  $\sim 20\times$  more cross-domain signal on this substrate; on a narrower substrate, F1’s load-bearingness might be different.

**Interrupted base pre-training.** The frozen base was originally planned to train through approximately step 143000. A UPS power-event interruption stopped pre-training at step 70000, and the project elected to ship the abbreviated base rather than restart. All ablations in this paper run against `base_step_70000.pt` and are therefore directly comparable *against each other* but *not* against a hypothetically longer-trained base. We expect that a longer-trained base would shift the absolute PPL numbers downward and may shift the relative attribution among F1, F2, F3; we make no claim about which direction.

**Adaptation horizon.** The 25000-step adaptation horizon is  $\approx 35\%$  of the pre-training horizon. With more adaptation steps, the lifecycle penalty could plausibly shrink (selection has more time to converge to a stable population), grow (mutation accumulates more drift), or invert (the base is small enough that adapters might saturate and inheritance blends might amortize). We do not have data to distinguish these.

**Three seeds.** All paired statistical tests in this paper run on  $n=3$  seeds with  $df=2$ . The choice of  $n=3$  was a budget-driven trade-off: each production cell costs 8–10 L40S-hours and the 5-cell factorial at  $n=3$  is already 15 runs ( $\sim 130$  GPU-hours) before the auxiliary Phase B and Fork 0 sweeps. We chose breadth (a five-cell partial factorial that decomposes the full system into three factors and runs two attribution chains) over within-cell precision (a smaller factorial at  $n \geq 5$  that would clear  $\alpha=0.05$  on the headline). The qualitative ordering of the three factors that this design recovers — F1 large and load-bearing, F2 null, F3 mildly anti-aligned — is robust under both attribution chains and under the partial factorial’s two consistency checks. The headline full-system-vs-B3 balanced contrast ( $t=1.94$ ,  $p=0.19$ ) does not clear  $\alpha=0.05$  at this  $n$ ; only the code-domain single-cell total clears it ( $t=10.42$ ,  $p=0.009$ ). With more seeds, the F3 lifecycle penalty ( $t= -4.46$ ,  $p=0.047$ ) could shift in either direction past the  $\alpha=0.05$  boundary. We are explicit about this in Section 5 and frame the lifecycle penalty as “mildly anti-aligned” rather than “decisively negative.”

**Eval-pipeline determinism.** The `StratifiedEvalLoader` (Section 3.2) cycles through per-domain shards deterministically given the configuration’s random seed. This is the correct fix for the alphabetical-shard bias in the legacy aggregate loader, but a side-effect is that the cross-seed variance of the balanced-PPL signal is deflated relative to a non-stratified evaluation: two runs at the same seed see exactly the same eval batches in the same order, so the only stochastic source contributing to seed variance is the training-time RNG. The Phase 2 internal report flags this as a deflation of cross-seed  $\sigma$  relative to what a fully randomized eval pipeline would produce. The interpretation knock-on is that the “B3 cross-seed range 0.2%” tightness reported in the cross-seed table partly reflects determinism in the eval pipeline, not just stability in the training dynamic. This determinism is the same root cause as the seed-constant biology and science per-domain PPLs flagged in the per-domain breakdown (Appendix D.6, Correction 9 of Appendix B): the eval-pipeline determinism is the proximate cause of both, and we do not report a per-domain paired- $t$  on biology or science as a result.

## 8.2 Internal validity of the attribution decomposition

**Partial factorial.** The factorial in Section 5 is 5-of-8. Three cells of the full  $2^3$  are not run: “router rewrite, aggregate scope, lifecycle off”; “router rewrite, aggregate scope, lifecycle on”; “B3 router, per-domain scope, lifecycle off.” We have two attribution chains that converge through C4, and they agree to within  $\sim 0.0004$  nats on the lifecycle penalty and  $\sim 0.0003$  nats on the router contribution, but a full  $2^3$  would also let us cleanly test for two-factor interactions (does F1 increase the size of the F3 penalty? does F2 modulate F1?). We treat the consistency of the two partial chains as evidence that two-factor interactions are small in this regime, but this is an inference, not a measurement.

**F1 is paired (gate function + routing input).** The F1 factor as run pairs two changes: the gate function (`softmax`  $\rightarrow$  `sigmoid_floor`) and the routing input (`embed_mean`  $\rightarrow$  `last_hidden`). The factorial cannot decompose F1 into these two sub-changes. The *paired* +0.0426 nat contribution attributed to F1 is therefore the joint effect of the rewrite and the input change. We list the four-cell sub-factorial that would isolate them as a planned follow-up (Section 9).

**F3 is bundled.** Similarly, F3 bundles death,  $\alpha$ -blend inheritance, SVD mutation, and slot reallocation. The original draft of this paper claimed that Phase B and Fork 0 jointly cleared the inheritance sub-component at the headline metric; under the corrected geometric-mean aggregator (Appendix B.11, Correction 10) that claim is retracted. The inheritance counterfactual at  $n=3$  is sign-inconsistent (+3.18% /  $-1.65\%$  / +0.20%, mean +0.56%) and underpowered for either an equivalence or a load-bearing conclusion. The residual penalty could be carried by death,  $\alpha$ -blend inheritance, mutation, reproduction, or some combination; the synthesis in Section 7.5 states this gap explicitly and the F3 sub-component decomposition is the highest-priority near-term follow-up (Section 9.2).

**Coalition probe is pre-rewrite only.** The cross-domain JS divergence = 0 result that motivates the coalition-monopoly framing in Section 6.1 was measured on the C1 router. We do not yet have the corresponding probe on the C3 or C4 routers post-rewrite. The per-domain uniformity in Table 9 is consistent with the rewrite having dissolved the monopoly, but is not a direct measurement of post-rewrite gate-distribution divergence. We list the post-rewrite coalition probe as a planned follow-up.

## 8.3 Scope of the synthetic-sandbox boundary

**One sandbox.** The synthetic boundary in Section 4 is characterized on a single, deliberately minimal sandbox: vocab 128, four disjoint slabs, deterministic bigram, hidden 512,  $K=16$ , top- $k=4$ . The oracle-alignment regime where ES is load-bearing is concretely the “adapters initialized at the per-slab oracle solution plus small noise” regime. We do not claim the boundary transfers quantitatively to the production substrate; the strongest production claim is the *direction*: a substrate that is not in the oracle-alignment regime should not be expected to benefit from ES on the routing channel, and the production-substrate F3 result is consistent with that direction.

**Hyperparameter selection.** The G7 small-sigma and G8 hybrid sweeps were run at a small set of  $\sigma$  values and ES/SGD interleaving schedules. We do not claim that no setting of  $\sigma$  or no schedule produces a positive ES result on this sandbox; only that the settings we tested all came out WRONG-DIRECTION or HARMFUL. Appendix B records a sign-convention error and an aggregation error (G7 and G8) that, once corrected, leave the verdict unchanged but whose existence is a flag that this regime is sensitive to careful reporting.

## 8.4 Residual measurement gaps in the auxiliary findings

**B.5 comparative leg blocked-measurement.** The within-checkpoint sample-size sweep in Section 7.1 reports a 1:13.8 within-checkpoint-to-cross-checkpoint ratio on the seed-42 baseline ( $\alpha=0.2$ ) checkpoint. The paired within-checkpoint sweep on the no-inherit ( $\alpha=0.0$ ) checkpoint is not available because the L40S Phase B job did not persist the no-inherit final adapter checkpoint. Until the run is repeated with checkpoint

persistence enabled, the comparative leg of the within-checkpoint test is missing, and the headline  $14\times$  ratio is a single-side number.

**B.6 Estimator C blocked-estimator-c.** The pre-specified noise-floor probe specified an across-checkpoint  $\sigma$  estimator using mid-training adapter snapshots at steps  $\{20000, 22500, 25000\}$ . No mid-training adapter snapshots exist anywhere recoverable: the training loop’s checkpoint hook writes only an end-of-training adapter, the W&B run holds metrics-only artifacts, and the Hub model repository holds only the final adapter and the 70k base. Per directive, no substitute proxy was constructed.

**Code-domain bimodal pattern ambiguous.** Two of three seeds (42 and 256) display a bimodal per-domain shift in the no-inherit counterfactual, where the code domain shifts by  $> 0.06$  nats while biology, general, and science remain within  $\pm 0.05$  nats. Seed 137 does not. We do not commit to a fork framing on this basis but flag it as a real, sub-headline pattern worth a follow-up at  $n \geq 5$ .

**Heir IDs not logged.** Phase A’s inheritance-versus-survival analysis used a `deaths_while_alive`  $\times \alpha$  upper bound as a proxy for inheritance received per adapter, because the lifecycle event JSONL does not record the heir ID at the per-death level. The nearest-neighbor heir is computed but not persisted. A small instrumentation patch would close this gap; we list it as a planned follow-up. The Phase A verdict (inheritance–survival correlation is age-confounded) is robust to this gap because both potential and realized inheritance are functions of birth time, but a direct test would close the inferential chain.

## 8.5 Things we explicitly do not claim

We do not claim that adapters in C3 or C4 have specialized to particular domains, that a particular adapter is a “code adapter” or a “biology adapter,” or that the post-rewrite routing pattern is cleanly per-domain interpretable. These claims would require the post-rewrite coalition probe and a per-adapter activation-by-domain analysis we have not yet run.

We do not claim that the lifecycle penalty is universal. We claim it holds at the configuration we ran (this substrate, 25000 steps,  $\alpha=0.2$ ,  $\sigma=0.01$  initial mutation, 1000-step lifecycle interval, 30% random-init reproduction fraction). The auxiliary inheritance counterfactual at  $n=3$  seeds is sign-inconsistent and underpowered for either an equivalence or a load-bearing conclusion (Section 7.1, Appendix B.11); we cannot, on this evidence, isolate which of inheritance, death, mutation, or reproduction carries the F3 penalty. We list the F3 sub-component decomposition crossed with the inheritance toggle as the highest-priority near-term follow-up.

We do not claim that mixture-of-LoRA evolution is unproductive in general. We claim that the particular evolutionary mixture-of-LoRA configuration we tested, on the particular production substrate we tested it on, has its balanced-aggregate win carried by a structural routing fix rather than by the evolutionary machinery. Other configurations may behave differently; a calibrated prior on which sub-mechanisms are most likely to carry value is the most we believe this paper supports.

## 9 Future work

The factorial in Section 5 answers the attribution question (which factor carries the win) at the resolution of the three factors F1/F2/F3, but the same machinery generates several follow-up questions that we have scoped but not yet executed. We list them here in the order in which they would most usefully sharpen the headline result, and we mark each with the limitation it closes (Section 8).

### 9.1 F1 sub-factorial: gate function vs. routing input

The F1 factor as run pairs two changes (Section 8.2): the gate function (`softmax`  $\rightarrow$  `sigmoid_floor`) and the routing input (`embed_mean`  $\rightarrow$  `last_hidden`). The four-cell sub-factorial that would isolate them is  $\{\text{softmax}, \text{sigmoid\_floor}\} \times \{\text{embed\_mean}, \text{last\_hidden}\}$ , run at  $n=3$  seeds at the same 25000-step adaptation horizon and the same widened-1536 substrate. The pre-specified hypotheses are: (i) the routing-input change carries

the bulk of the F1 gain, because the in-code measurement of cross-domain signal is  $\sim 20\times$  stronger on `last_hidden`; (ii) the gate-function change is near-null on its own at `embed_mean` but unlocks the `last_hidden` signal by relaxing the coalition-monopoly constraint; (iii) the two changes interact super-additively. The sub-factorial is four cells  $\times$  3 seeds = 12 runs at the same per-cell budget as the core factorial.

## 9.2 F3 sub-component decomposition (highest near-term priority)

The F3 factor as run bundles four sub-mechanisms: death (per-adapter fitness-driven kill),  $\alpha$ -blend inheritance (slot release into nearest neighbor), SVD mutation (heritable singular-value perturbation), and slot reallocation (random-init versus parental-clone reproduction). The Phase B and Fork 0 results (Section 7) under the corrected geometric-mean aggregator do *not* rule out inheritance as the load-bearing source of the  $-0.028$  nat penalty: the seed-42 cell shifts balanced PPL by  $+3.18\%$  (load-bearing range), the cross-seed mean is  $+0.56\%$  (ambiguous band), and the  $n=3$  paired- $t$  does not clear  $\alpha=0.05$  in either direction. The penalty could be carried by death,  $\alpha$ -blend inheritance, mutation, reproduction, or a combination; we no longer have grounds for pre-promoting any single sub-mechanism. This sub-factorial is the highest near-term priority of the planned follow-ups.

The pre-specified cell list is the partial  $2^3$  over {death on/off, mutation on/off, reproduction warm/cold} run at *both*  $\alpha=0.0$  and  $\alpha=0.2$  (a  $\sim 10$ -cell design that crosses the inheritance toggle with the partial  $2^3$ ),  $n=3$  seeds per cell at the same 25000-step budget, with the checkpoint hook (Section 9.6) enabled on every cell so the within-checkpoint diagnostics extend cleanly. The pre-specified hypothesis is updated to treat death, mutation, reproduction, and inheritance as roughly equal candidates rather than predicting any single sub-mechanism as the most-likely contributor. The decision rule is per-factor: a sub-mechanism is LOAD-BEARING if toggling it on/off produces a balanced log-PPL shift  $\geq 0.02$  nats (the magnitude of the F3 main effect) in the seed-mean and the paired- $t$  on per-seed deltas clears  $\alpha=0.05$ . We will dispatch this sub-factorial regardless of the F1 sub-factorial outcome, because the F3 attribution is the component that the recent corrigendum has reopened.

## 9.3 Post-rewrite coalition probe

The cross-domain Jensen–Shannon divergence = 0 result that motivates the coalition-monopoly framing in Section 6.1 was measured on the C1 router. We do not yet have the corresponding probe on the C3 or C4 routers post-rewrite. The probe is cheap: load the rewrite-router checkpoint, forward a held-out per-domain micro-batch, dump the per-token post-floor sigmoid mass per adapter, compute per-domain top- $k$  gate distributions, and compute pairwise JS between domains. The pre-specified hypothesis is that the post-rewrite JS is bounded *away* from 0 by a margin that scales with the per-domain hidden-state separability, and that the per-domain margin correlates with the per-domain PPL improvement reported in Table 9. This closes the “coalition probe is pre-rewrite only” limitation in Section 8.2.

## 9.4 Heir-ID instrumentation for direct inheritance test

Phase A’s inheritance-versus-survival analysis used a `deaths_while_alive`  $\times \alpha$  upper bound as a proxy for inheritance received per adapter, because the lifecycle event JSONL does not record the heir ID at the per-death level (Section 8.4). A small instrumentation patch in the lifecycle hook — emit the heir adapter ID alongside each death event, and aggregate per-adapter `nats_received` as the  $\alpha$ -weighted sum over received deaths — closes the inferential chain. With heir IDs logged, the Phase A regression of survival on realized inheritance becomes a direct test rather than a bounding argument. The pre-specified hypothesis (consistent with the existing age-confound finding) is that the partial correlation of survival on realized inheritance, controlling for age and birth-step, is indistinguishable from zero.

## 9.5 More seeds for code-domain bimodal closure

Two of three Fork 0 seeds (42 and 256) display a bimodal per-domain shift in the no-inherit counterfactual; seed 137 does not (Section 8.4). At  $n=3$  the verdict is AMBIGUOUS. We will replicate at  $n=5$  (adding seeds 7 and 512) to determine whether the code-domain shift is a  $2/3$  artifact or a genuine  $\sim 67\%$  replicate rate.

The replication budget is five runs at the no-inherit cell only ( $\alpha=0.0$ ), at the same 25000-step horizon. The pre-specified decision rule:  $\geq 4/5$  seeds with code-domain  $|\Delta \log \text{PPL}_{\text{code}}| \geq 0.06$  nats  $\Rightarrow$  REPLICATES;  $\leq 2/5 \Rightarrow$  DOES-NOT-REPLICATE;  $3/5 \Rightarrow$  retain AMBIGUOUS and report at the auxiliary-finding tier.

## 9.6 Re-run Phase B with persisted no-inherit checkpoint

The B.5 within-checkpoint sample-size sweep on the no-inherit  $\alpha=0.0$  checkpoint is currently BLOCKED-MEASUREMENT (Section 8.4) because the L40S Phase B job did not persist the no-inherit final adapter checkpoint. The fix is the training-loop checkpoint hook: save the final adapter on every cell, not only on the seed-42 baseline. The re-run is one cell at  $n=3$  seeds at the same 25000-step horizon, with the checkpoint hook enabled. With the no-inherit checkpoint persisted, the within-checkpoint sweep matches the seed-42 baseline sweep methodology, and the comparative 1:13.8 ratio becomes a paired comparison rather than a single-side number.

## 9.7 Mid-training adapter snapshots for Estimator C

The pre-specified noise-floor probe (B.6) specified an across-checkpoint  $\sigma$  estimator using mid-training adapter snapshots at steps  $\{20000, 22500, 25000\}$ , currently BLOCKED-ESTIMATOR-C because no mid-training adapter snapshots exist (Section 8.4). The fix is a periodic checkpoint hook in the training loop: every  $K$  steps after step  $\sim 5000$ , write a full adapter snapshot. The retrofit cost is one-time:  $\sim 50$  checkpoints  $\times \sim 100$  MB each  $\sim 5$  GB per cell, well within the production-substrate storage budget. We schedule this hook for the F1 sub-factorial run and the F3 sub-component run, both of which would otherwise relaunch without the snapshots.

## 9.8 Cross-substrate transfer of the synthetic boundary

The synthetic-sandbox boundary in Section 4 is characterized on a single, deliberately minimal sandbox. The most external-validity-extending follow-up is to repeat the G4–G8 cell battery on a second sandbox that varies one of the substrate dimensions (vocabulary size, slab count, hidden width,  $K/\text{top-}k$ ). A pre-specified prediction: the G4 oracle-alignment regime continues to PASS (ES carries the routing gain), G5/G6 continue to be inert or worse, and G7/G8 continue to be WRONG-DIRECTION/HARMFUL, with quantitative magnitudes shifting but the qualitative regime boundary preserved. A failure of this prediction would tighten the boundary; a confirmation would strengthen the substrate-conditional claim.

## 9.9 Out of scope

We explicitly do not list as planned follow-ups: (i) a state-of-the-art mixture-of-LoRA result on a strong pretrained base (Pythia/Llama/Mistral); the abbreviated 70000-step from-scratch base is the wrong substrate for that comparison, and the result would not sharpen this paper’s attribution claim. (ii) a continuous-lifecycle “daemon” that runs the lifecycle loop between training sessions; this is the Horizon-2 vision documented in the project’s internal roadmap but is outside the scope of an attribution paper. (iii) a domain-interpretability analysis (which adapter is the “code adapter,” etc.); this requires the post-rewrite coalition probe above and a per-adapter activation-by-domain analysis we have not yet run, and the headline result does not depend on per-adapter domain assignment.

## References

- Immanuel Abdi, Akshat Gupta, Micah Mok, Alexander Lu, et al. Evolutionary strategies lead to catastrophic forgetting in LLMs, 2026. URL <https://arxiv.org/abs/2601.20861>.
- Takuya Akiba, Makoto Shing, Yujin Tang, Qi Sun, et al. Evolutionary optimization of model merging recipes, 2024. URL <https://arxiv.org/abs/2403.13187>. Nature Machine Intelligence 2024.
- Sina Alemohammad, Josue Casco-Rodriguez, Lorenzo Luzi, Ahmed Imtiaz Humayun, Hossein Babaei, Daniel LeJeune, Ali Siahkoohi, and Richard G. Baraniuk. Self-consuming generative models go mad, 2023. URL <https://arxiv.org/abs/2307.01850>. ICLR 2024.

- João Abrantes, Robert Tjarko Lange, and Yujin Tang. Competition and attraction improve model fusion, 2025. URL <https://arxiv.org/abs/2508.16204>. introduces M2N2; GECCO 2025.
- Ali Behrouz, Meisam Razaviyayn, Peilin Zhong, and Vahab Mirrokni. Nested learning: The illusion of deep learning architectures, 2025. URL <https://arxiv.org/abs/2512.24695>. NeurIPS 2025.
- William Fedus, Barret Zoph, and Noam Shazeer. Switch transformers: Scaling to trillion parameter models with simple and efficient sparsity, 2021. URL <https://arxiv.org/abs/2101.03961>.
- Shangbin Feng, Zifeng Wang, Palash Goyal, Yike Wang, et al. Heterogeneous swarms: Jointly optimizing model roles and weights for multi-LLM systems, 2025. URL <https://arxiv.org/abs/2502.04510>.
- Peter Henderson, Riashat Islam, Philip Bachman, Joelle Pineau, Doina Precup, and David Meger. Deep reinforcement learning that matters, 2018. URL <https://arxiv.org/abs/1709.06560>. AAAI 2018.
- Edward J. Hu, Yelong Shen, Phillip Wallis, Zeyuan Allen-Zhu, Yuanzhi Li, Shean Wang, Lu Wang, and Weizhu Chen. Lora: Low-rank adaptation of large language models, 2021. URL <https://arxiv.org/abs/2106.09685>.
- Jie Huang, Xinyun Chen, Swaroop Mishra, Huaixiu Steven Zheng, Adams Wei Yu, Xinying Song, and Denny Zhou. Large language models cannot self-correct reasoning yet, 2024. URL <https://arxiv.org/abs/2310.01798>. ICLR 2024.
- Max Jaderberg, Valentin Dalibard, Simon Osindero, Wojciech M. Czarnecki, Jeff Donahue, Ali Razavi, Oriol Vinyals, Tim Green, Iain Dunning, Karen Simonyan, Chrisantha Fernando, and Koray Kavukcuoglu. Population based training of neural networks, 2017. URL <https://arxiv.org/abs/1711.09846>.
- Daria Korotyshova, Boris Shaposhnikov, Alexey Malakhov, Alexey Khokhulin, et al. Essa: Evolutionary strategies for scalable alignment, 2025. URL <https://arxiv.org/abs/2507.04453>.
- Ramchand Kumaresan. KALAVAI: Predicting when independent specialist fusion works – a quantitative model for population-based LLM training, 2026. URL <https://arxiv.org/abs/2603.22755>.
- So Kuroki, Taishi Nakamura, Takuya Akiba, and Yujin Tang. Agent skill acquisition for large language models via CycleQD, 2024. URL <https://arxiv.org/abs/2410.14735>. ICLR 2025.
- Joel Lehman, Jay Chen, Jeff Clune, and Kenneth O. Stanley. Es is more than just a traditional finite-difference approximator, 2018. URL <https://arxiv.org/abs/1712.06568>. GECCO 2018.
- Dengchun Li, Yingzi Ma, Naizheng Wang, Zhengmao Ye, Zhiyuan Cheng, Yinghao Tang, Yan Zhang, Lei Duan, Jie Zuo, Cal Yang, and Mingjie Tang. Mixlora: Enhancing large language models fine-tuning with lora-based mixture of experts, 2024. URL <https://arxiv.org/abs/2404.15159>.
- Qiyao Liang, Jinyeop Song, Yizhou Liu, Jeff Gore, et al. The blessing of dimensionality in LLM fine-tuning: A variance-curvature perspective, 2026. URL <https://arxiv.org/abs/2602.00170>.
- Joelle Pineau, Philippe Vincent-Lamarre, Koustuv Sinha, Vincent Larivière, Alina Beygelzimer, Florence d’Alché Buc, Emily Fox, and Hugo Larochelle. Improving reproducibility in machine learning research (a report from the neurips 2019 reproducibility program), 2020. URL <https://arxiv.org/abs/2003.12206>.
- Xin Qiu, Yulu Gan, Conor F. Hayes, Qiyao Liang, et al. Evolution strategies at scale: Llm fine-tuning beyond reinforcement learning, 2025. URL <https://arxiv.org/abs/2509.24372>.
- Tim Salimans, Jonathan Ho, Xi Chen, Szymon Sidor, and Ilya Sutskever. Evolution strategies as a scalable alternative to reinforcement learning, 2017. URL <https://arxiv.org/abs/1703.03864>.
- Bidipta Sarkar, Mattie Fellows, Juan Agustin Duque, Alistair Letcher, et al. Evolution strategies at the hyperscale, 2025. URL <https://arxiv.org/abs/2511.16652>. introduces the EGGROLL low-rank-structured ES method.

Kenneth O. Stanley, Jeff Clune, Joel Lehman, and Risto Miikkulainen. Designing neural networks through neuroevolution. *Nature Machine Intelligence*, 1(1):24–35, 2019. doi: 10.1038/s42256-018-0006-z.

Qi Sun, Edoardo Cetin, and Yujin Tang. Transformer-squared: Self-adaptive LLMs, 2025. URL <https://arxiv.org/abs/2501.06252>. ICLR 2025; introduces SVF.

Yujin Tang, Yingtao Tian, and David Ha. Evojax: Hardware-accelerated neuroevolution, 2022. URL <https://arxiv.org/abs/2202.05008>.

Yanqi Zhou, Tao Lei, Hanxiao Liu, Nan Du, Yanping Huang, Vincent Zhao, Andrew Dai, Zhifeng Chen, Quoc Le, and James Laudon. Mixture-of-experts with expert choice routing, 2022. URL <https://arxiv.org/abs/2202.09368>. NeurIPS 2022.

Barret Zoph, Irwan Bello, Sameer Kumar, Nan Du, Yanping Huang, Jeff Dean, Noam Shazeer, and William Fedus. St-moe: Designing stable and transferable sparse expert models, 2022. URL <https://arxiv.org/abs/2202.08906>.

## A Reproducibility footprint

This appendix reproduces the full hyperparameter inventory, per-cell run identifiers, configuration JSON paths, and the data and tokenizer artifacts required to reproduce every numerical claim in the main text. Per the source-of-truth conventions in Section 3.3, each entry points at a single source-of-truth file rather than a summary mirror.

### A.1 Substrate

- **Base architecture.** GPT-style decoder, hidden size  $D=1536$ , 12 layers, 16 attention heads, feed-forward width  $4D$ , sequence length 1024, vocabulary size  $V=32000$ . Total  $\sim 150M$  parameters.
- **Base tokenizer.** BPE,  $V=32000$ , trained on the domain-mixed pre-train corpus (tokenized\_mixed32k\_b2). Tokenizer artifact at `data/tokenizer_mixed32k/`.
- **Base pre-train corpus.** Domain-mixed across biology, code, general text, and science, tokenized to the `mixed32k_b2` layout in `data/tokenized_mixed32k_b2/`.
- **Frozen base checkpoint.** `checkpoints/base_model_trackb_b2_dv1536/base_step_70000.pt`. Pre-train was halted at step 70000 owing to a UPS power-event interruption (originally planned through step  $\sim 143000$ ); see Section 8.1.

### A.2 LoRA adapter inventory

- LoRA adapters injected at every transformer block on `{query_key_value, dense, dense_h_to_4h, dense_4h_to_h}`.
- Rank  $r=8$ ,  $\alpha=16$ , dropout 0.0.
- Static population size  $P=16$ , sparse top- $k=4$ .
- Adapter optimizer: AdamW, learning rate  $10^{-4}$ ,  $\beta_1=0.9$ ,  $\beta_2=0.999$ , weight decay 0.0, gradient clip 1.0.
- Router optimizer: decoupled AdamW, learning rate  $10^{-5}$ , same  $\beta$  and weight-decay defaults.
- Adaptation horizon: 25000 steps for each cell.

### A.3 Lifecycle hyperparameters

For cells that include the lifecycle (C2, C5, C4 in the main-text factorial):

- Inheritance blend  $\alpha=0.2$  (C4 baseline);  $\alpha=0.0$  for the no-inherit Phase B counterfactual.
- Initial mutation rate  $\sigma=0.01$  on SVD-aligned singular values, heritable.
- Lifecycle event interval: every 1000 training steps after warmup.
- Lifecycle warmup: 2000 steps before the first event.
- Reproduction: 30% random-init, 70% parental-clone with mutation, slot-by-slot.
- Death gate: per-adapter LOO fitness on a held-out micro-batch, bottom-1 killed per event.
- Maximum age: effectively unbounded (999999 steps) for the 25000-step adaptation horizon.

### A.4 Router hyperparameters

For cells that include the router rewrite (C3, C5, C4):

- Gate function: parallel sigmoid with no row-renormalization.
- Per-adapter learnable floor, initialized at  $\text{logit}^{-1}(-2.944) \approx 0.05$ .
- Temperature anneal:  $T_0=2.0 \rightarrow T_{\text{final}}=0.5$  linearly over the first 1500 steps, then held at 0.5 for the remainder of training.
- Routing input: post-stack hidden states (`last_hidden`), not token-embedding mean (`embed_mean`).

### A.5 Per-cell configuration JSONs

The five run cells of the main-text factorial each have a configuration JSON in `experiments/trackb_b2/`:

- **C1 (b3 base)**: `b3_trackb_b2_dv1536_25k_seed42_e8_domainshift.json` and seed-clones at `{137, 256}` (Fork 0 cross-seed sweep).
- **C2 (b3 + lifecycle)**: configured by lifting the `lifecycle_*` block from C4 onto the C1 base; specifically via the `lifecycle_eval_scope=AGGREGATE` flag.
- **C5 (B3 routing + per-domain LOO + lifecycle)**: B3 router (softmax over adapters with `embed_mean` input), per-domain LOO scope, lifecycle on with  $\alpha=0.2$  inheritance. Configured by lifting the `lifecycle_*` block from C4 and the `lifecycle_eval_scope=PER_DOMAIN` flag onto the C1 base; the router is the C1 (B3) softmax router.
- **C3 (b3 routing rewrite + per-domain LOO, no lifecycle)**: the same router-rewrite flags as C5 but with the lifecycle disabled.
- **C4 (full evolutionary system,  $\alpha=0.2$ )**: `uyir_trackb_b2_dv1536_25k_seed42_e8_domainshift.json` and seed-clones at `{137, 256}`.

The Phase B no-inherit cell (C4 with  $\alpha=0.0$ ) lifts only the `inheritance_alpha` field from C4. The Phase B job did not persist the no-inherit final adapter checkpoint (Section 8.4); the configuration JSON is preserved in `experiments/trackb_b2/` but the within-checkpoint diagnostic on this cell is `BLOCKED-MEASUREMENT`.

## A.6 Random seeds and replicate count

All cells run at  $n=3$  seeds: {42, 137, 256}. The Fork 0 sweep replicates the C1 and C4 cells at the same three seeds. The  $n=5$  replication for the code-domain bimodal AMBIGUOUS verdict (Section 9.5) would add seeds 7 and 512 but is not in the current paper.

## A.7 Compute footprint

Production-substrate cells run on a single L40S GPU. Per-cell wall time at 25000 steps and the above hyperparameters is approximately 8–10 hours; the full 5 cells  $\times$  3 seeds = 15 production runs in the core factorial total  $\sim$  130 GPU-hours, plus the 4-run Fork 0 seed sweep ( $\sim$  35 GPU-hours). Synthetic-sandbox cells run on a single GPU at  $\sim$  5–15 minutes each.

## A.8 Software environment

- Python 3.10+, PyTorch 2.2+.
- No HuggingFace dependency in the production-substrate path: the base model is a pure-PyTorch GPT with manual LoRA injection.
- Eval pipeline: `StratifiedEvalLoader` at git 6b00021 or later. The pre-fix alphabetical shard ordering bug is documented in Section 3.2.
- All numerical claims in the main text are cross-checked against the analysis JSONs in `experiments/trackb_b2/analysis/`.

## A.9 Run-identifier table

The per-cell W&B run identifiers and analysis-JSON paths for all 19 production runs (15 core factorial + 4 Fork 0 seed sweep) are listed in the supplementary materials. Per-seed PPLs and per-domain breakdowns are reproduced in Appendix D; the cross-seed B3 cell state is reproduced in Appendix E; the synthetic full tables (G4–G8 per-seed) are reproduced in Appendix C.

## B Verification corrections log

This appendix logs the corrections applied during paper preparation as a transparency artifact. Each entry lists the source-of-truth file, the corrected value, and the downstream claim affected. The log is presented in the order the corrections were applied. Two corrections were applied during paper drafting — (i) a one-row shift in the Phase 3 stepwise table in an internal results summary, and (ii) a misattribution of the C4–C1 (full evolutionary system vs B3) per-domain  $t$ -statistics to the C1 vs C3 contrast in the per-domain breakdown table of Appendix D.6 — and are recorded as entries 8 and 9 below.

### B.1 TL;DR table

### B.2 Correction 1: G7 sign convention

**Source of truth.** `experiments/phase05_es_router/warmstart_smallsigma_results.json` holds per- $\sigma$  post-warmup loss values. The convention used by the JSON is *loss-positive-is-bad*: `delta_warm = mean - warmup_mean`, with positive values indicating regression. **Drift point.** The summary in `experiments/phase05_es_router/RESULTS.md` (Phase 0.6+ small-sigma section) and downstream notes quoted the deltas as negative ( $-0.467$ ,  $-0.238$ , etc.), which under the surrounding prose’s “regresses by” phrasing implied an improvement, the opposite of what the data show. **Correction.** The magnitudes are correct; the signs are positive (regression from warmup baseline). The verdict `WRONG-DIRECTION` is unchanged. **Impact on paper.** Section 4 reports G7 with the sign-corrected convention.

#	Correction	Corrected value
1	G7 sign convention pinned to JSON	sign positive (regression above warm baseline)
2	G8 SGD-tail descent re-aggregated as paired- $t$	0.0203 nats, $t=1.65$ , $df=4$ , $p > 0.05$
3	Code-domain seed-42 statistic re-derived as paired- $t$ at $n=3$	$t=10.42$ , $p=0.009$ , $df=2$
4	Phase B summary aggregator standardized to geometric mean	$\sim 0.2\%$ shift on balanced
5	Phase 2 plan reference config corrected to stationary B3	wrong-substrate launch averted
6	B.5 within-checkpoint diagnostic missing no-inherit checkpoint	blocked
7	B.6 Estimator C blocked: no mid-training adapter snapshots	blocked
8	Phase 3 stepwise attribution table re-derived from per-seed JSON	main-text numbers from JSON, not summary mirrors
9	Per-domain $C1$ vs $C3$ table re-derived from JSON	biology/science paired- $t$ dropped (seed-constant p)
10	Phase B Table 10 balanced row was arithmetic mean despite “geom.” label	recomputed: seed-42 shift +3.18% (was +0.06%)

Table 13: Verification corrections log. Each entry was applied during paper preparation; the corrected value column states the value used in the body. None of the corrections originated in the analysis JSONs; all originated in summary mirrors (RESULTS.md, STATUS.md, project notes) or in draft text.

### B.3 Correction 2: G8 SGD-tail descent

**Source of truth.** experiments/phase05\_es\_router/hybrid\_es\_results.json. Phase A val\_loss 4.7136, Phase B (ES then SGD) final loss 4.6933, descent = 0.0203. **Drift point.** A summary in RESULTS.md reported the SGD-tail descent as 0.004 nats, an under-aggregation by approximately  $5\times$ . **Correction.** The descent is 0.0203 nats. The verdict HARMFUL is unchanged because the relevant comparison is to the pure-SGD baseline descent, which remains larger. **Impact on paper.** Section 4 reports G8 with the correctly-aggregated number.

### B.4 Correction 3: code-domain seed-42 statistic re-derived as paired- $t$

**Source of truth.** experiments/trackb\_b2/analysis/sweep\_ppl\_matrix.json for per-seed PPLs; experiments/trackb\_b2/analysis/zscore\_rederivation.md for the re-derivation. **Correction.** The appropriate test for the seed-42 code-domain shift on the cross-seed sample of three seeds is a paired- $t$  on per-seed log-PPL deltas:  $t=10.42$ ,  $p=0.009$ ,  $df=2$  (code-domain single-cell), and  $t=1.94$ ,  $p=0.19$ ,  $df=2$  (headline full-system-vs-B3 balanced contrast). **Impact on paper.** The balanced headline does not clear  $\alpha=0.05$  at  $n=3$ ; only the code-domain single-cell does. The full re-derivation is in Appendix D.

### B.5 Correction 4: Phase B aggregator standardized to geometric mean

**Source of truth.** experiments/trackb\_b2/analysis/sweep\_ppl\_matrix.json. **Correction.** All rows use geometric-mean balanced-PPL,  $PPL_{\text{balanced}} = \exp(\frac{1}{4} \sum_d \log PPL_d)$ . **Impact on paper.** The cross-seed full-system vs. B3 contrast direction is unchanged; the magnitude shifts by approximately 0.2%. The STATE-C (direction-consistent, magnitude-collapsing, not-significant-at- $n=3$ ) verdict from the Phase 2 report is preserved.

### B.6 Correction 5: Phase 2 plan reference config standardized

**Source of truth.** The pre-launch Phase 2 plan referenced uyir\_trackb\_b2\_dv1536\_25k\_seed42\_e8\_domainshift.json (full evolutionary system + e8-domainshift) where the stationary B3 config was intended. **Correction.** The plan was rewritten to use the stationary B3 config before launch. **Impact on paper.** The two seed-clones ran on the intended stationary substrate.

### B.7 Correction 6: B.5 within-checkpoint diagnostic blocked

**Source of truth.** experiments/trackb\_b2/analysis/phaseB\_within\_checkpoint.md. **Correction.** The Phase B job did not persist the no-inherit ( $\alpha=0.0$ ) final adapter checkpoint, so the paired within-checkpoint diagnostic against the seed-42 baseline cannot be run. The headline 1:13.8 ratio is reported as a single-side

number; the diagnostic is labeled BLOCKED-MEASUREMENT pending a re-run with checkpoint persistence enabled. **Impact on paper.** Section 7.1 flags the blocked status; the fix is a checkpoint-hook patch, scheduled in Section 9.6.

### B.8 Correction 7: B.6 Estimator C blocked

**Source of truth.** `experiments/trackb_b2/analysis/phaseB_estimator_c.md`. **Correction.** The pre-specified noise-floor probe specified mid-training adapter snapshots at  $\{20000, 22500, 25000\}$ , but no such snapshots exist anywhere recoverable: the training loop’s checkpoint hook writes only an end-of-training adapter, and the W&B and Hub artifacts hold only metrics or end-of-training adapters. No substitute proxy was constructed; Estimator C is labeled BLOCKED-ESTIMATOR-C. **Impact on paper.** Section 7.1 flags the blocked status; the fix is a periodic-snapshot patch, scheduled in Section 9.7.

### B.9 Correction 8: Phase 3 stepwise table re-derived from JSON

**Source of truth.** `experiments/trackb_b2/analysis/phase3_attribution_results.json`. **Correction.** The main-text Section 5 table re-derives the per-step contributions directly from the JSON rather than from the internal results-summary mirror. **Impact on paper.** The cited F1 (+0.0426 nats), F2 (null at seed-resolution), and F3 (−0.028 nats) numbers are taken from the JSON.

### B.10 Correction 9: per-domain C1 vs C3 table re-derived from JSON

**Source of truth.** `experiments/trackb_b2/analysis/phase3_attribution_results.json`, specifically the per-cell per-seed `domain_ppl` block of the manifest entries for the C1 and C3 cells (`manifest.{C1_b3_base,C3_sigfloor_lasthidden_perdom_nolife}.{42,137,256}.domain_ppl`) for the per-seed per-domain raw PPLs. **Correction.** The per-domain breakdown table in Appendix D.6 reports seed-mean PPL columns sourced from the JSON manifest and relative improvements computed from those means (−3.08/−7.27/−2.82/−3.83% for biology / code / general / science). A paired- $t$  statistic is reported only for the code domain, which is the only domain on which the per-seed per-domain PPLs vary across all three seeds in both C1 and C3. The biology and science per-seed PPLs are seed-constant in both cells (a property of the deterministic `StratifiedEvalLoader` ordering combined with the precision at which per-domain PPLs are recorded in the manifest; the same eval-determinism root cause discussed in Section 8.1), so the paired- $t$  denominator on those two domains is zero and we make no claim of significance for them. The general-domain per-seed PPL varies on only one of three seeds in C3, so the reported general-domain  $t$ -statistic is retained for completeness with a footnote flagging its degenerate variance, but we treat code as the only robust per-domain paired- $t$  conclusion. **Impact on paper.** All four domains improve at the seed-mean level under the C1 vs C3 contrast, and the code domain improves the most. The body of the paper makes no claim of statistical significance for biology, science, or general at the per-domain level; only the code-domain  $t=10.96$ ,  $p=0.008$  enters the headline.

### B.11 Correction 10: Phase B balanced aggregator recomputed as geometric mean

**Source of truth.** The per-cell, per-seed, per-domain PPLs in `experiments/trackb_b2/analysis/phase3_attribution_results.json` (specifically the `C4_full_uyir_alpha02` cell for the seed-42  $\alpha=0.2$  baseline, and the per-domain entries in `experiments/trackb_b2/analysis/fork0_diagnostic_report.md` for the seed-42  $\alpha=0.0$  no-inherit cell).

**Drift point.** Table 10 of the original draft labeled the balanced row “balanced (geom.)” but populated it with the arithmetic mean of the four per-domain PPLs, 16.151 for the  $\alpha=0.2$  baseline and 16.161 for the  $\alpha=0.0$  no-inherit cell, giving a +0.06% shift. Section 3.2 pins balanced PPL as the geometric mean  $\exp(\frac{1}{4} \sum_d \log \text{PPL}_d)$ ; the row label was correct, the values were not.

**Correction.** The geometric mean of  $\{21.049, 3.436, 23.852, 16.266\}$  is 12.943 (matching the `C4_full_uyir_alpha02` → seed 42 entry in `phase3_attribution_results.json`); the geometric mean of

{20.723, 3.986, 23.667, 16.266} is 13.354. The corrected seed-42 balanced shift is  $13.354/12.943 - 1 = +3.18\%$  (+0.0313 nats), not +0.06%. Under the pre-specified Phase B decision rule (Section 7.1), shifts  $> 2\%$  trigger the *load-bearing* verdict on the cell to which they apply.

**Cross-seed recomputation.** Applying the same correction to the Fork 0 seed sweep: under the pinned aggregator, the per-seed balanced log-PPL shift (mean across the four per-domain  $\Delta \log \text{PPL}$  entries in Table 11) is +0.0313 nats on seed 42, -0.0166 nats on seed 137, and +0.0020 nats on seed 256, corresponding to balanced-PPL shifts of +3.18%, -1.65%, and +0.20% respectively. The cross-seed mean is +0.56% (+0.0056 nats), and the paired- $t$  on those three deltas is  $t \approx 0.38$ ,  $p \approx 0.74$  (df=2, two-sided), failing to clear  $\alpha=0.05$  in either direction. The three seeds are sign-inconsistent at the headline metric.

**Impact on paper.** The original draft’s headline “+0.06% shift, inheritance NOT load-bearing at the headline metric” depended on the arithmetic-mean error and is retracted. Section 7 (chapter intro and Section 7.1) is rewritten to report the corrected seed-42 shift, the cross-seed sign-inconsistency, and the underpowered paired- $t$ . Section 7.5 is rewritten to retract the “inheritance not load-bearing” synthesis and to treat the four F3 sub-mechanisms (death,  $\alpha$ -blend inheritance, SVD mutation, slot reallocation) as roughly equal candidates rather than pre-clearing inheritance. Section 9.2 is rewritten to promote the F3 sub-component decomposition — crossed with the inheritance toggle — to the highest near-term priority. The abstract and the Section 1 “What” bullets are softened to a sign-inconsistent / underpowered framing.

## B.12 Scope of the verification protocol

The verification protocol described above catches errors of transcription and computation, not errors of experimental design. Section 8 catalogs the open external-validity and internal-validity questions on this paper’s claims.

## C Synthetic-sandbox full tables

This appendix reproduces the per-seed and per-cell numbers underlying the synthetic-sandbox boundary in Section 4. The sandbox is described at the top of that section; we reproduce only the substrate parameters needed to interpret the tables here, then provide the per-cell breakdowns.

### C.1 Sandbox substrate

- Vocabulary  $V=128$ , four disjoint domain slabs of 32 tokens each, deterministic bigram conditional within each slab.
- Hidden width 512,  $K=16$  adapters, top- $k=4$  sparse routing.
- Adapter rank  $r=4$ ,  $\alpha=8$ .
- Routing input options: `embed_mean` (default for the legacy router) or `last_hidden`.
- Loss: per-token cross-entropy on the held-out micro-batch.

### C.2 G4 oracle-alignment cell

**Setup.** Adapters initialized at the per-slab oracle solution plus small noise; ES on the routing channel only with  $\sigma=10^{-1}$ ; SGD on the routing channel only as the contrast.

### C.3 G5 joint random-init cell

**Setup.** Adapters and router both initialized at random; ES on the joint parameters versus SGD on the joint parameters. Both reach the random-adapter floor  $\approx \log V = \log 128 \approx 4.852$  within tolerance.

Seed	ES routing-loss closed (frac)	SGD routing-loss closed (frac)	Verdict
0	0.559	0.002	PASS
1	0.557	0.001	PASS
2	0.561	0.003	PASS
mean	0.559	0.002	PASS

Table 14: G4 ES vs. SGD on the oracle-alignment cell. ES closes  $\approx 55.9\%$  of the routing-channel gap; SGD closes  $\approx 0.2\%$ . The SGD ceiling is the top- $k$  non-differentiability.

Seed	ES final loss (nats)	SGD final loss (nats)	Verdict
0	4.853	4.851	TIE-AT-FLOOR
1	4.854	4.851	TIE-AT-FLOOR
2	4.852	4.852	TIE-AT-FLOOR

Table 15: G5 joint random-init cell. Both methods reach the random-adapter floor  $\approx \log V$ ; neither method extracts adapter-side signal.

#### C.4 G6 gradient-warm cell

**Setup.** Adapters and router warmed up under SGD for  $K_{\text{warm}}$  steps, then ES is allowed to perturb the routing channel only.

Seed	ES post-warm $\Delta$ (nats)	SGD post-warm $\Delta$ (nats)	Verdict
0	-0.001	-0.014	INERT
1	+0.001	-0.013	INERT
2	-0.000	-0.012	INERT

Table 16: G6 gradient-warm cell. ES is inert on the warm-started substrate; SGD continues to descend slowly on the routing channel.  $\Delta$  is improvement (negative = loss decreased).

#### C.5 G7 small-sigma sweep

**Setup.** Sigma sweep  $\sigma \in \{10^{-5}, 10^{-4}, 5 \times 10^{-4}, 10^{-3}\}$  on the warm-started substrate,  $n=5$  seeds per cell, mode `es_coupled`. Sign convention: `delta_warm = mean - warmup_mean`, positive = regression above warm baseline.

#### C.6 G8 hybrid ES-then-SGD

**Setup.** Phase A pure ES on the routing channel; Phase B SGD on all parameters. SGD-tail descent measured as the loss reduction during Phase B, conditional on the Phase A outcome.

## D Phase 3 attribution re-derivation

This appendix re-derives the per-cell PPLs, attribution chains, and paired- $t$  statistics cited in Section 5 directly from the per-seed JSON. The re-derivation is intentionally explicit so an external reader can falsify our claims against the JSON we ship in the supplement.

The cell labels and factor assignments follow Section 5.2 (Table 3):

- C1: B3 router, aggregate-LOO scope, no lifecycle (anchor).
- C2: B3 router, aggregate-LOO scope, lifecycle on (isolates F3).

$\sigma$	seed 0	seed 1	seed 2	seed 3	seed 4	mean	verdict
$10^{-5}$	+0.4334	+0.5822	+0.5226	+0.4362	+0.3618	+0.4673	WRONG-DIRECTION
$10^{-4}$	+0.4105	+0.5076	+0.5351	+0.4376	+0.4006	+0.4583	WRONG-DIRECTION
$5 \times 10^{-4}$	+0.3842	+0.4748	+0.2705	+0.3351	+0.3139	+0.3557	WRONG-DIRECTION
$10^{-3}$	+0.2484	+0.2707	+0.2768	+0.2029	+0.1901	+0.2378	WRONG-DIRECTION

Table 17: G7 small-sigma sweep on the warm-started substrate ( $n=5$  seeds, mode `es_coupled`). All  $\sigma$  values produce regression from the warm baseline. Magnitudes are monotone in  $\sigma$  (smaller  $\sigma$  produces larger regression — ES at very low noise fails to escape the random-adaptor floor that the warm SGD baseline has already left behind); the sign convention follows the JSON (loss-positive-is-bad), as recorded in Appendix B.2. Body §4 reports these mean values; the per-seed columns above are the source-of-truth backing those means.

Seed	Phase A val_loss	Phase B (ES then SGD) final	SGD-tail descent
0	4.7136	4.6933	0.0203
1	4.7129	4.6940	0.0189
2	4.7142	4.6929	0.0213
mean	4.7136	4.6934	0.0202

Table 18: G8 hybrid ES-then-SGD. The SGD-tail descent is  $\approx 0.020$  nats, re-derived from the per-seed JSON (Appendix B.3). The verdict `HARMFUL` is assigned because the pure-SGD baseline closes more of the routing gap than the ES-then-SGD hybrid does.

- C5: B3 router, per-domain LOO scope, lifecycle on (isolates F2 given F3).
- C3: rewrite router, per-domain LOO, no lifecycle (combined F1+F2 without F3).
- C4: rewrite router, per-domain LOO, lifecycle on (full evolutionary system,  $\alpha=0.2$ ).

### D.1 Per-cell balanced-PPL table

Cell	seed 42	seed 137	seed 256	geom-mean across seeds
C1 (B3 baseline)	13.328	13.341	13.354	13.341
C2 (B3 + lifecycle)	13.538	13.805	13.832	13.725
C5 (B3 + per-dom + lifecycle)	13.564	13.778	13.805	13.715
C3 (rewrite + per-dom, no lifecycle)	12.742	12.830	12.742	12.771
C4 (full evolutionary system, $\alpha=0.2$ )	12.943	13.173	13.315	13.143

Table 19: Per-seed and geom-mean balanced PPL by cell. Numbers reproduce Table 4 of the main text. Balanced PPL is  $\exp(\frac{1}{4} \sum_d \log \text{PPL}_d)$  over  $d \in \{\text{biology, code, general, science}\}$ , sourced from `experiments/trackb_b2/analysis/phase3_attribution_results.json`.

### D.2 Per-cell log-PPL table

The paired- $t$  tests in the main text act on per-seed log-PPL deltas:

### D.3 Primary attribution chain $C1 \rightarrow C2 \rightarrow C5 \rightarrow C4$

The primary chain isolates one factor per step. Sign convention  $\Delta = \log \text{PPL}_{\text{ref}} - \log \text{PPL}_{\text{test}}$  (positive = improvement).

**Step  $C1 \rightarrow C2$  (F3 lifecycle alone).**  $\Delta = \log \text{PPL}_{C1} - \log \text{PPL}_{C2}$  on per-seed mean log-PPL:  $-0.0283$ . Per-seed  $\Delta$ : seed 42  $-0.0156$ ; seed 137  $-0.0342$ ; seed 256  $-0.0351$ . Paired- $t$  on per-seed  $\Delta$ :  $t = -4.46$ ,  $p = 0.047$ ,  $\text{df}=2$ .

Cell	seed 42 log PPL	seed 137 log PPL	seed 256 log PPL	mean
C1	2.5900	2.5910	2.5920	2.5910
C2	2.6056	2.6252	2.6271	2.6193
C5	2.6076	2.6232	2.6252	2.6187
C3	2.5450	2.5519	2.5450	2.5473
C4	2.5607	2.5783	2.5890	2.5760

Table 20: Per-seed log PPL<sub>balanced</sub> by cell, computed from Table 19 to four decimal places.

**Step  $C2 \rightarrow C5$  (F2 per-domain LOO scope, given F3 on).**  $\Delta = \log \text{PPL}_{C2} - \log \text{PPL}_{C5}$  on per-seed mean log-PPL: +0.0007. The sign is inconsistent across seeds (negative on seed 42, positive on seeds 137 and 256). Paired- $t$ :  $t = 0.50$ ,  $p = 0.67$ . F2 is null at seed-resolution.

**Step  $C5 \rightarrow C4$  (F1 router rewrite, given F2 and F3 on).**  $\Delta = \log \text{PPL}_{C5} - \log \text{PPL}_{C4}$  on per-seed mean log-PPL: +0.0426. Paired- $t$ :  $t = 12.86$ ,  $p = 0.006$ ,  $\text{df}=2$ . The router rewrite is the load-bearing factor.

#### D.4 Consistency attribution chain $C1 \rightarrow C3 \rightarrow C4$

The consistency chain combines F1+F2 in a single step, then layers F3.

**Step  $C1 \rightarrow C3$  (F1 router + F2 scope, no lifecycle).**  $\Delta = +0.0436$  on per-seed mean log-PPL; paired- $t$   $t = 18.58$ ,  $p = 0.003$ ,  $\text{df}=2$ .

**Step  $C3 \rightarrow C4$  (F3 lifecycle layered on full router + scope).**  $\Delta = -0.0287$ ; paired- $t$   $t = -3.47$ ,  $p = 0.074$ ,  $\text{df}=2$ .

#### D.5 Two-chain convergence

The two chains agree to within 0.0004 nats on the lifecycle penalty and 0.0003 nats on the router contribution:

$$\begin{aligned} \text{primary total } C1 \rightarrow C4 &: -0.0283 + 0.0007 + 0.0426 = +0.0150, \\ \text{consistency total } C1 \rightarrow C4 &: +0.0436 + (-0.0287) = +0.0149. \end{aligned}$$

The total full-system-vs-B3 balanced contrast on per-seed mean log-PPL is +0.0150, paired- $t$   $t = 1.94$ ,  $p = 0.19$ ,  $\text{df}=2$ . The total does not clear  $\alpha=0.05$  at  $n=3$ .

#### D.6 Per-domain breakdown of the C1 vs. C3 contrast

Disaggregating the C1 vs. C3 contrast (router-rewrite-plus-per-domain no-lifecycle minus B3 baseline) by domain:

#### D.7 Code-domain attribution chain

Repeating the entire factorial on code-domain log-PPL alone reproduces Table 8 of the main text:

- Primary chain:  $C2 - C1 = -0.0378$  (lifecycle,  $t = -5.21$ ,  $p = 0.035$ );  $C5 - C2 = +0.0026$  (per-dom scope,  $t = 1.00$ ,  $p = 0.42$ );  $C4 - C5 = +0.0976$  (router rewrite,  $t = 25.14$ ,  $p = 0.0016$ ).
- Consistency chain:  $C3 - C1 = +0.0755$  (router + scope no lifecycle,  $t = 10.96$ ,  $p = 0.008$ );  $C4 - C3 = -0.0130$  (lifecycle on,  $t = -3.75$ ,  $p = 0.064$ ).
- Total  $C4 - C1 = +0.0625$ ,  $t = 10.42$ ,  $p = 0.009$ .

Domain	C1 PPL (seed-mean)	C3 PPL (seed-mean)	rel. improvement	paired- $t$ , $p$
biology	21.0495	20.4018	-3.08%	—
code	3.7010	3.4319	-7.27%	$t = 10.96$ , $p = 0.008$
general	24.2278	23.5438	-2.82%	$t = 11.00$ , $p = 0.008^\dagger$
science	16.7821	16.1392	-3.83%	—

Table 21: Per-domain breakdown of the C1 vs. C3 contrast (router rewrite + per-domain LOO scope, no lifecycle, vs. B3 anchor), re-derived from per-seed per-domain PPLs in `phase3_attribution_results.json`. All four domains improve at the seed-mean level; the code domain improves the most. We report a paired- $t$  statistic only for the code domain, which is the only domain on which the per-seed per-domain PPLs vary across all three seeds in both C1 and C3. The biology and science per-seed PPLs are seed-constant in both cells (a property of the deterministic `StratifiedEvalLoader` ordering combined with the precision at which per-domain PPLs are recorded in the manifest; Section 8.1), so the paired- $t$  denominator on those domains is zero and we make no claim of significance for them (“—”). <sup>†</sup>General-domain per-seed PPLs vary on only one of three seeds in C3, so the reported general-domain  $t=11.00$  should be read with that degenerate variance in mind; we report it for completeness but treat code as the only robust per-domain conclusion.

The two chains agree on the code domain to a thousandth of a nat:  $+0.0755 + (-0.0130) = +0.0625$  vs.  $-0.0378 + 0.0026 + 0.0976 = +0.0624$ .

## D.8 Code-domain paired- $t$ at $n=3$

The appropriate test for the seed-42 code-domain shift on the cross-seed sample of three seeds is a paired- $t$  on per-seed log-PPL deltas, not a  $z$ -score against a cross-seed standard deviation estimated at  $n=3$  with the seed-42 numerator included in the sample (which contaminates the denominator and inflates the ratio). The paired- $t$  on the code-domain  $C4 - C1$  deltas across the three seeds is  $t = 10.42$ ,  $p = 0.009$ ,  $df=2$  (the code-domain entry of Appendix D.7 above). The magnitude on the code domain remains the strongest single-cell result in the paper. The full derivation, including the bootstrap CI on  $\sigma$  that illustrates the  $n=3$  sample contamination of the alternative  $z$ -score, is in `experiments/trackb_b2/analysis/zscore_rederivation.md`.

## E Phase 2 cross-seed B3 state

This appendix reproduces the Phase 2 cross-seed B3 baseline state and the STATE-A/STATE-B/STATE-C verdict that locked the Phase 3 attribution chain.

### E.1 Pre-specified states

The Phase 2 plan pre-specified three possible states the cross-seed B3 vs. full-system data could land in:

**state-a — cross-seed win.** B3 at the additional seeds 137, 256 lands at  $\sim 13.4$ – $13.6$  balanced PPL, the full-system-vs-B3 delta holds or strengthens across seeds. The strongest possible paper.

**state-b — single-seed win.** B3 at 137, 256 lands at or below the full-system per-domain LOO. The seed-42 win is a lottery; the paper retreats to a narrower claim.

**state-c — trajectory-conditional / direction-consistent, magnitude-collapsing, not-significant-at- $n=3$ .** Mixed pattern across seeds. The paper becomes a substrate/trajectory characterization rather than a clean win.

Cell	seed 42 PPL	seed 137 PPL	seed 256 PPL	geom-mean	cross-seed range
B3	13.328	13.340	13.354	13.341	0.2%
C4 ( $\alpha=0.2$ , full system)	12.943	13.172	13.315	13.142	2.83%

Table 22: Cross-seed per-domain LOO PPLs at the three seeds for the B3 (static MoE) cell and the C4 full-evolutionary-system cell at  $\alpha=0.2$ . The B3 cell is tight across seeds (range 0.2%); the C4 cell is approximately  $14\times$  looser (range 2.83%), which the Phase 2 report flags as deflation of cross-seed variance partly attributable to eval-pipeline determinism (Section 8.1).

## E.2 Cross-seed table

## E.3 Verdict

The Phase 2 final report assigns STATE-C: the direction is consistent (the full system has lower PPL than B3 at all three seeds in the per-domain LOO comparison), but the magnitude collapses toward zero at the additional seeds and the headline full-system-vs-B3 balanced contrast does not clear  $\alpha=0.05$  at  $n=3$ :

- **Headline full-system-vs-B3 balanced contrast:** paired- $t$   $t = 1.94$ ,  $p = 0.19$  (df=2).
- **Code-domain single-cell:** paired- $t$   $t = 10.42$ ,  $p = 0.009$  (df=2).
- **Verdict:** STATE-C, direction-consistent, magnitude-collapsing, not-significant-at- $n=3$ .

The STATE-C verdict is the basis for the main text’s framing of the F3 lifecycle penalty as “mildly anti-aligned” rather than “decisively negative.”

## E.4 Bridge to the main-text Phase 3 attribution

With the Phase 2 cross-seed verdict locked at STATE-C, the Phase 3 attribution chain decomposes the observed  $\sim 1.5\%$  balanced-PPL improvement (full system vs. B3 at seed-42) into the F1, F2, F3 contributions reported in the main text. Specifically, the attribution chain attributes the entire balanced-PPL win to the F1 router rewrite (+0.0426 nats) and locates a net F3 lifecycle penalty ( $-0.028$  nats), with the net cross-seed full-system-vs-B3 contrast collapsing toward zero on the headline metric at the additional seeds. The main text’s framing is therefore consistent with the STATE-C verdict: the routing fix is the load-bearing contribution; the lifecycle is a net drag; and the headline balanced-PPL win, taken at face value at  $n=3$ , is not statistically significant at  $\alpha=0.05$  even though it is direction-consistent across all three seeds.